NASA MEMO 5-24-59L

NASA

MEMORANDUM

A SIMPLE METHOD FOR DETERMINING HEAT TRANSFER, SKIN FRICTION, AND BOUNDARY-LAYER THICKNESS FOR HYPERSONIC LAMINAR BOUNDARY-LAYER FLOWS IN A PRESSURE GRADIENT

By Mitchel H. Bertram and William V. Feller

Langley Research Center
Langley Field, Va.

NATIONAL AERONAUTICS AND SPACE ADMINISTRATION
WASHINGTON
June 1959

NATIONAL AERONAUTICS AND SPACE ADMINISTRATION

MEMORANDUM 5-24-59L

A SIMPLE METHOD FOR DETERMINING HEAT TRANSFER, SKIN FRICTION, AND BOUNDARY-LAYER THICKNESS FOR HYPERSONIC LAMINAR BOUNDARY-LAYER FLOWS IN A PRESSURE GRADIENT

By Mitchel H. Bertram and William V. Feller

SUMMARY

A procedure based on the method of similar solutions is presented by which the skin friction, heat transfer, and boundary-layer thickness in a laminar hypersonic flow with pressure gradient may be rapidly evaluated if the pressure distribution is known. This solution, which at present is restricted to power-law variations of pressure with surface distance, is presented for a wide range of exponents in the power law corresponding to both favorable and adverse pressure gradients.

This theory has been compared to results from heat-transfer experiments on blunt-nose flat plates and a hemisphere cylinder at free-stream Mach numbers of 4 and 6.8. The flat-plate experiments included tests made at a Mach number of 6.8 over a range of angle of attack of $\pm 10^{\circ}$. Reasonable agreement of the experimental and theoretical heat-transfer coefficients has been obtained as well as good correlation of the experimental results over the entire range of angle of attack studied. A similar comparison of theory with experiment was not feasible for boundary-layer-thickness data; however, the hypersonic similarity theory was found to account satisfactorily for the variation in boundary-layer thickness due to local pressure distribution for several sets of measurements.

INTRODUCTION

With the assumptions of an incompressible fluid and similarity in the velocity profiles through the boundary layer, an exact solution of the boundary-layer equations may be obtained. The assumption of similarity leads to a power-law distribution of velocity at the edge of the boundary layer with surface distance. This solution was pointed out by

Falkner and Skan (ref. 1) and improved calculations were made by Hartree (ref. 2) and Smith (ref. 3). Cohen and Reshotko (ref. 4) considered also similarity in the temperature profiles and extended the results to the compressible case.

Utilizing the transformations of Illingworth (ref. 5) or Stewartson (ref. 6), various investigators have given solutions of the compressible boundary-layer problem. These solutions given in references 4, 7, and 8, in general, are exact only for the case of a Prandtl number of 1. However, the solutions given in reference 7 give an assessment of the effect of Prandtl number.

Li and Nagamatsu (ref. 9) have shown the pressure gradient parameter β for the incompressible problem can be simply related to the pressure gradient in compressible flow if hypersonic and isentropic flow are assumed to exist at the edge of the boundary layer. Li and Nagamatsu, however, used this relation to solve only the special case of a boundary-layer self-induced pressure gradient. It is the purpose of the present analysis to show the general usefulness of the hypersonic transformation for predicting viscous effects on wing surfaces. Preliminary results from this investigation were reported in reference 10.

SYMBOLS

A,B,C,D coefficients in equations from zeroeth-order strong-interaction theory (see eqs. (17) to (20))

$C_w = \dfrac{\mu_w T_\infty}{\mu_\infty T_w}$

$C' = \dfrac{\mu' T_\infty}{\mu_\infty T'}$

C_f local skin-friction coefficient including effect of pressure gradient, $\dfrac{2\tau}{\rho_\infty u_\infty^2}$

C_F average skin-friction coefficient including effect of pressure gradient

c_p specific heat at constant pressure

d model diameter

f function related to stream function

h local heat-transfer coefficient including effect of pressure gradient

H_s local stagnation enthalpy

H_0 free-stream stagnation enthalpy

K_1, K_2, K_3, K_4 coefficients defined in equations (7) to (10)

L length of plate

M Mach number

N_{Pr} Prandtl number

$N_{St,\infty}$ Stanton number including effect of pressure gradient, $\frac{h}{c_{p,\infty}\rho_\infty u_\infty}$

n exponent in equation for pressure variation with x (see eq. (2))

p pressure

$p_{w,L}$ local surface pressure at length L

$R_{\infty,x}$ undisturbed-free-stream Reynolds number with x as characteristic length, $\frac{\rho_\infty u_\infty}{\mu_\infty} x$

S enthalpy function, $\frac{H_s}{H_0} - 1$

T absolute temperature

t model thickness

u velocity

x distance along surface in stream direction

β pressure-gradient parameter in the notation of reference 4

γ ratio of specific heat at constant pressure to that at constant volume

τ	shear stress at wall
δ	boundary-layer thickness
ρ	density
η	similarity variable
σ	Reynolds analogy factor
μ	dynamic viscosity

Subscripts:

b	conditions over plate following blunt nose
r	recovery conditions
L	value at chord length of plate
w	wall
0	free-stream stagnation
∞	undisturbed free stream

Primes denote differentiation with respect to η or parameters evaluated by T-prime method.

Bars denote values of the parameter obtained on a plate with zero pressure gradient.

THEORY

Evaluation of Basic Parameters

Li and Nagamatsu (ref. 9) have shown that the pressure-gradient parameter β can be related to pressure gradient in the physical plane by a simple relation if hypersonic and isentropic flow at the edge of the boundary layer are assumed. This relation is

$$\beta = \frac{1 - \gamma}{\gamma} \frac{n}{n + 1} \tag{1}$$

where in the physical plane

$$p_w \propto x^n \tag{2}$$

Lees (ref. 11) had previously given the special case of this solution where $n = -1/2$ or $\beta = (\gamma - 1)/\gamma$ in relation to the asymptotic solution for the strong-interaction boundary-layer self-induced pressure gradient. Li and Nagamatsu also only considered in detail the case $n = -1/2$.

Following the analysis of Li and Nagamatsu (ref. 9) for hypersonic flow, Prandtl number equal to 1 and with n in general, the laws for skin friction, heat transfer, and boundary-layer thickness can be written as follows: For local skin friction

$$\frac{C_f}{\overline{C_f}} = K_1 \sqrt{\frac{p_w}{p_\infty}} \tag{3}$$

For average skin friction

$$\frac{C_F}{\overline{C_F}} = K_2 \sqrt{\frac{p_{w,L}}{p_\infty}} \tag{4}$$

For heat transfer

$$\frac{h}{\overline{h}} = K_3 \sqrt{\frac{p_w}{p_\infty}} \tag{5}$$

For boundary-layer thickness

$$\frac{\delta}{\overline{\delta}} = \frac{K_4}{\sqrt{p_w/p_\infty}} \tag{6}$$

where the symbols with bars represent the values for the case in which the pressure gradient is zero. (The derivation of equations (3) to (6) is given in appendix A.)

A comparison of equations (3) to (6) with equations (4) to (8) of reference 12 shows that the square root of the pressure ratio appearing herein is really a correction to account for local conditions different from the reference conditions in the undisturbed stream. The coefficients K account for the effect of pressure gradient itself, and their deviation from unity is thus a measure of the importance of this gradient apart from the effect of changes in local conditions.

The coefficients K are:

$$K_1 = f_w'' \frac{\sqrt{2(1+n)}}{0.664} \tag{7}$$

$$K_2 = \frac{f_w''}{0.332\sqrt{2(1+n)}} \tag{8}$$

$$K_3 = -\frac{S_w'}{S_w} \frac{\sqrt{2(1+n)}}{0.664} \tag{9}$$

$$K_4 = \frac{\frac{2}{\sqrt{2(1+n)}} \int_0^\infty (S + 1 - f'^2)d\eta}{\sqrt{2}\left[\int_0^\infty (S + 1 - f'^2)d\eta\right]_{\beta=0}} \tag{10}$$

The values of the zero-pressure-gradient parameters used in the derivation of equations (3) to (6) were (Prandtl number unity):

$$\bar{C}_f\sqrt{\frac{R_{\infty,x}}{C_w}} = 0.664 \tag{11}$$

$$\bar{C}_F\sqrt{\frac{R_{\infty,L}}{C_w}} = 1.328 \tag{12}$$

$$\bar{N}_{St,\infty}\sqrt{\frac{R_{\infty,x}}{C_w}} = \frac{\bar{h}}{c_p\rho_\infty u_\infty}\sqrt{\frac{R_{\infty,x}}{C_w}} = 0.332 \tag{13}$$

$$\frac{\bar{\delta}}{x}\sqrt{\frac{R_{\infty,x}}{C_w}} = \frac{\gamma - 1}{2} M_\infty^2\sqrt{2}\left[\int_0^\infty (S + 1 - f'^2)d\eta\right]_{\beta=0} \tag{14}$$

Values of the integral function in equation (14) were obtained from the following equation (suggested by eq. (2.10) of ref. 13) which utilizes the accurate constants for $S_w = 0$ and $\beta = 0$ given in reference 3.

$$\sqrt{2}\left[\int_0^\infty (S + 1 - f'^2)d\eta\right]_{\beta=0} = 1.72078(S_w + 1) + 0.66412 \tag{15}$$

The available values of f_w'', S_w'/S_w, and the integral function are given in table I. These values are also plotted in figures 1 to 3 for completeness. Most of the values of the integral function given in table I were obtained by the simple addition of the values of the dimensionless displacement and momentum thicknesses given in table II of reference 4 and table VI of reference 3. Where table II of reference 4 was not complete a method used in reference 3 was found adaptable for obtaining accurate values of this integral. For the present problem the integral may be stated as

$$\int_0^\infty \left(S + 1 - f'^2\right)d\eta = \lim_{\eta_1 \to \infty} \left(\frac{\int_0^{\eta_1} S \, d\eta + \eta_1 - f_1 f_1' - f_1'' + f_w''}{1 + \beta} \right) \tag{16}$$

The values of $\int_0^{\eta_1} S \, d\eta$ were obtained by Simpson's rule from table I of reference 4.

Values of the integral function (eq. (16)) for $\beta = 0.286$ and 0.400 are given in reference 9. Other values were obtained from a mechanical integration of tabulated boundary-layer properties given in reference 8. Where a value of f_w'', S_w'/S_w, or the integral function had not been computed, the faired lines shown in figures 1, 2, and 3 were used for the computations presented in this paper.

Some interesting general results concerning the laws for the variation of local and average skin friction, heat transfer, and boundary-layer thickness with distance along the plate may be obtained from equations (3) to (6) with the condition of equation (2). One finds that

$$C_f \propto h \propto x^{\frac{n-1}{2}}$$

$$C_F \propto L^{\frac{n-1}{2}}$$

$$\delta \propto x^{\frac{1-n}{2}}$$

When one examines the law for boundary-layer growth, the exponent in the boundary-layer-growth law as a function of the exponent in the pressure variation law is as follows:

n	$\frac{1 - n}{2}$
-2/3	5/6
-1/2	3/4
-1/3	2/3
0	1/2
1/3	1/3
1/2	1/4
2/3	1/6
1	0
2	-1/2

The case of $n = 0$ is of course the constant-pressure flat plate on which the boundary-layer growth follows a parabolic law. With falling pressures (favorable pressure gradients, n negative), the rate of growth of the boundary layer is greater than on a constant-pressure plate. For rising pressures (adverse pressure gradients, n positive), the rate of growth of the boundary layer is less than on a constant-pressure plate. When the rate of increase of pressure with distance from the leading edge offsets the shearing forces, the boundary-layer thickness is constant over the entire plate and for still higher adverse pressure gradients the boundary layer thins as the distance from the leading edge increases. The preceding remarks apply only when the boundary-layer solutions are real which occurs only when

$$\beta > -\frac{(\gamma - 1)}{\gamma}$$

This is shown in the following sketch which is a graphic expression of equation 1.

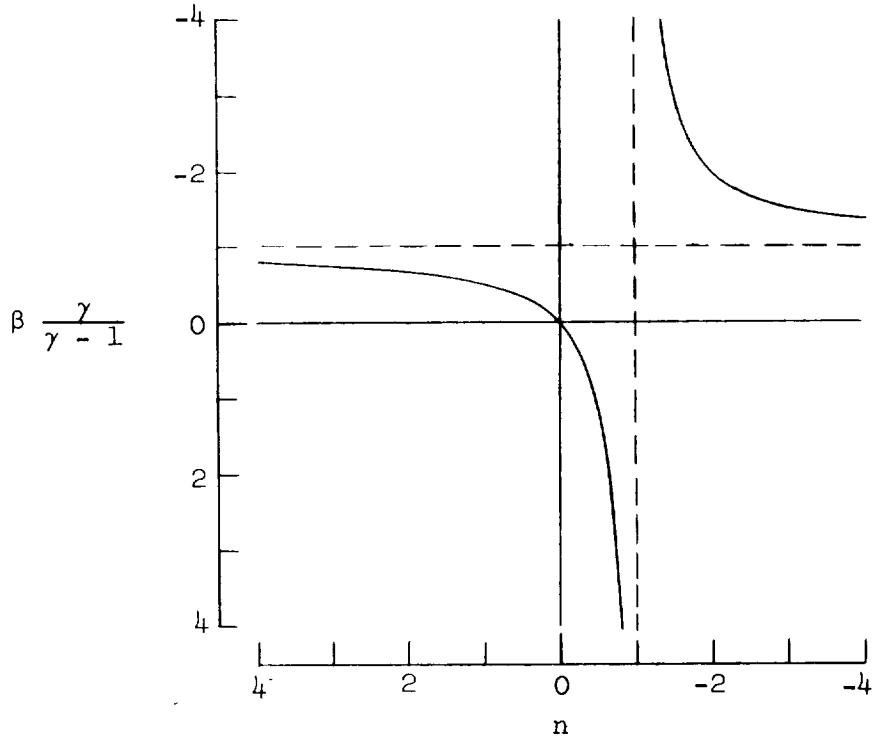

All values of $\beta\gamma/(\gamma - 1)$ which are less than -1 result in values of the exponent n of less than -1, and in these cases the results from equations (7) to (10) will be imaginary.

Comparison of Air and Helium

By use of equation (1), values of n corresponding to values of β were obtained for ratios of specific heats γ of 7/5 and 5/3 and the coefficients K_1, K_2, K_3, and K_4 were evaluated. These coefficients are shown as a function of n for both favorable and adverse pressure gradients in figures 4 to 7. Thus, for a known pressure variation behaving as a power law with respect to physical distance along a plate the change in skin friction, heat transfer, and boundary-layer thickness in hypersonic flow can be readily found.

These values of the coefficients K reveal several interesting results concerning a comparison between hypersonic flow in air and helium environments. For favorable pressure gradients, the effects of a given pressure gradient in air and helium are predicted to be very similar for the same temperature and pressure ratios. This is evident in figures 4(a), 5(a) and (b), 6(a) and (b), and 7(a) for local and average skin friction, heat transfer, and boundary-layer thickness.

In the case of small adverse pressure gradients (rising pressures) again the results from air and helium are basically similar (figs. 4(b) and (c), 5(c) and 5(d), 6(c) and (d), and 7(b) and (c)). However, as the adverse pressure gradient increases there is an increasing deviation between the predictions for air and helium. This deviation is perhaps most easily shown by referring to the value of n at which separation occurs. For example, refer to figures 4(b) and (c) and the temperature ratios of 2, 1, and 0.6 ($K_1 = 0$ indicates separation). Note the large differences in the values of n for separation between air and helium for these temperature ratios.

The indications from this theory are that the value of γ is important in determining the effect of large adverse pressure gradients; however, the significance of this result is not clear since it is probable that certain assumptions inherent in the derivation will be violated in large adverse pressure gradients - such as, for example, that the flow is isentropic and locally hypersonic at the edge of the boundary layer.

For temperature ratios of 0 and 0.2, the solutions for $\gamma = 5/3$ with an adverse pressure gradient are real for all values of β; however, this is not the case for $\gamma = 7/5$ where an imaginary solution is encountered for $\beta < -2/7$. (See the discussion in the previous section.)

Effect of γ in General for Favorable Pressure Gradient

Figure 8 presents calculations of the coefficients K for values of γ ranging from 1 to 2 for two values of the pressure-law exponent n in favorable pressure gradients. In order to show the effect of temperature, the insulated-wall case and the case of a wall with zero temperature are shown.

One finds that the coefficients K_1 and K_2 in the skin-friction equations are sensitive to γ when the temperature is close to the insulated-wall value but that the sensitivity to variation in γ is much reduced when the wall temperature approaches zero.

The coefficients K_3 and K_4 in the heat-transfer and boundary-layer thickness equations are found to be relatively insensitive to both changes in wall temperature and γ.

Hypersonic Self-Induced Pressure Gradient on a Flat Plate

(Strong-Interaction Solution)

Various investigators have shown that the asymptotic solution for the case of large boundary-layer-induced pressures yields a behavior of the pressures with distance from the leading edge of a flat plate of the form $p \propto x^{-1/2}$. Thus, this problem as discussed in reference 8 may be treated as a particular example of the hypersonic similar solutions. (A survey of this aspect of the hypersonic-interaction problem generally referred to as zeroeth-order strong-interaction theory is given in references 9, 12, and 14.) If this approach of Li and Nagamatsu (ref. 9) is used, the induced pressure ratio, boundary-layer thickness, local skin-friction coefficient, and local heat-transfer characteristics can be written as:

$$\frac{p_w}{p_\infty} = A \frac{M_\infty^3 \sqrt{C_w}}{\sqrt{R_{\infty,x}}} \tag{17}$$

$$\frac{\delta}{x}\sqrt{\frac{R_{\infty,x}}{C_w}} = B M_\infty^2 \left(\frac{\sqrt{R_{\infty,x}}}{M_\infty^3 \sqrt{C_w}}\right)^{1/2} \tag{18}$$

$$\frac{C_{f,\infty}\sqrt{R_{\infty,x}}}{\sqrt{C_w}} = C\left(\frac{M_\infty^3 \sqrt{C_w}}{\sqrt{R_{\infty,x}}}\right)^{1/2} \tag{19}$$

$$\frac{N_{St,\infty}\sqrt{R_{\infty,x}}}{\sqrt{C_w}} = D\left(\frac{M_\infty^3 \sqrt{C_w}}{\sqrt{R_{\infty,x}}}\right)^{1/2} \tag{20}$$

With equation (17), equations (18) to (20) can be seen to be a special form of equations (3) to (6). The coefficients A, B, C, and D are given by the following equations which are included for convenience:

$$A = \frac{9}{4}\left(\frac{\gamma - 1}{3}\right)\left(\frac{\gamma(\gamma + 1)}{2}\right)^{1/2} \left[\int_0^\infty (S + 1 - f'^2)\, d\eta\right]_{\beta = \frac{\gamma-1}{\gamma}} \tag{21}$$

$$B = 2\left(\frac{\gamma - 1}{3}\right)^{1/2}\left(\frac{2}{\gamma(\gamma + 1)}\right)^{1/4}\left[\int_0^\infty (S + 1 - f'^2)d\eta\right]^{1/2}_{\beta = \frac{\gamma-1}{\gamma}} \tag{22}$$

$$C = \frac{3}{2}\left(\frac{\gamma - 1}{3}\right)^{1/2}\left(\frac{\gamma(\gamma + 1)}{2}\right)^{1/4}\left\{f_w''\left[\int_0^\infty (S + 1 - f'^2)d\eta\right]^{1/2}\right\}_{\beta = \frac{\gamma-1}{\gamma}} \tag{23}$$

$$D = \frac{3}{4}\left(\frac{\gamma - 1}{3}\right)^{1/2}\left(\frac{\gamma(\gamma + 1)}{2}\right)^{1/4}\left\{\left(-\frac{S_w'}{S_w}\right)\left[\int_0^\infty (S + 1 - f'^2)d\eta\right]^{1/2}\right\}_{\beta = \frac{\gamma-1}{\gamma}} \tag{24}$$

The coefficients A, B, C, and D are plotted in figure 9 as a function of the ratio of wall temperature to stagnation temperature for various values of the ratio of specific heats γ. Three values of γ are shown - that is, values that correspond to helium, air, and an arbitrary value of $\gamma = 1.2$. Actually a fourth point may be deduced since for $\gamma = 1$, $A = B = C = D = 0$ for all wall temperatures. This figure extends the values given in reference 9 and corrects the values of D in reference 9 which are too high by a factor of 2.

EXPERIMENT AND THEORY FOR THE HEAT TRANSFER TO PLATES WITH BLUNT LEADING EDGES

A case of considerable practical interest is the plate with a blunt leading edge in which the blunt leading edge can generate large pressure gradients on the following plate (refs. 10 and 15). If the leading edge is sufficiently thick in relation to the boundary layer, the boundary layer will be submerged in the high entropy layer adjacent to the plate, and the restriction of the theory to constant entropy along the edge of the boundary layer may be considered to be satisfied; however, there is difficulty with the restriction to locally hypersonic flow. In the region of the juncture between the nose and, say, a following slab at zero inclination to the free-stream flow, the local Mach

number is low (local M about 2 or 2.5). The local Mach number increases as the flow moves downstream over the plate; however, with a free-stream Mach number of, for example, about 40 the local M far downstream on the plate is only 6 to 8 if the boundary layer is still assumed to be submerged in the high entropy layer.

Experimental heat-transfer information on blunt-nose configurations at Mach numbers of about 4 to 7 is available in references 16 and 17. In addition new data have been obtained at a Mach number of 6.8 on a hemicylinder-nose slab from tests in the 11-inch hypersonic tunnel.

Experimental Apparatus

Tunnel and test conditions.- The experiments were conducted in the Langley 11-inch hypersonic tunnel, which is a blowdown facility. The two-dimensional nozzle with a nominal Mach number of 7 had contours machined from Invar. Some calibration data for the Invar nozzle may be found in reference 18 and a description of the tunnel, in reference 19.

The Mach number was between 6.76 and 6.81 for the heat-transfer data and 6.81 and 6.86 for the pressure data. The lowest Mach number was obtained at the lowest test unit Reynolds number. The slightly different Mach number levels for the heat transfer and pressure data are attributable to the small increase in Mach number with time during the length of a test run. Heat-transfer data were obtained from the transient temperatures near the start of a test run by a quick starting technique which approximates the sudden immersion of the model in a fully developed test-section flow. Pressure data were obtained about 40 seconds after the start of flow in order to eliminate lag in the pressure tubing and cells as a source of error. The data were obtained at an average stagnation temperature of about 1,140° R.

Models and instrumentation.- The model used for the investigation of the surface pressure and heat transfer was the slab with a hemicylindrical leading edge shown in figure 10. The same model was used to obtain both pressures and temperatures with the pressure orifices and thermocouples being located on opposite walls of the model. A single sheet of 1/16-inch-thick Inconel formed the skin of the model. The diameter of the hemicylindrical leading edge was 3/4 inch and the overall length of the plate was 6 inches. The properties of Inconel given in reference 20 were used in evaluating the heat-transfer data.

The skin temperatures were obtained from chromel-alumel thermocouples formed from No. 30 wire. The thermocouple wires were welded together to form a bead which was inserted in a hole in the surface and welded in place with Inconel.

Surface pressures were measured by means of the aneroid-type six-cell recording units described in reference 19.

Comparison of Heat-Transfer Theory With Experiment

Knowledge of the pressure distribution is of course important in determining the heat-transfer distribution. For present purposes, in order to free the heat-transfer theory of the additional source of error contained in an attempt to predict the pressure distribution, the measured pressure distributions were used. In order to satisfy the requirements of hypersonic boundary-layer similarity theory, power laws were fitted to the measured pressure distributions. The top plots of figures 11(a) and (b) show the measured pressures and the type of fit to a power-law variation that was obtained.

The flat-plate ($dp/dx = 0$) value of the Stanton number may be obtained by any preferred method. In the present analysis, the T-prime method and the modified Reynolds analogy were applied to the Blasius skin-friction value to obtain the correlating parameter:

$$N_{St,\infty}\sqrt{R_{\infty,x}} = \frac{0.332\sqrt{C'}}{\sigma_\infty} \tag{25}$$

where $C' = (\mu_\infty' T_\infty)/(\mu_\infty T_\infty')$ and the Reynolds analogy factor $\sigma_\infty = N_{Pr}^{2/3}$ evaluated at T_∞' (the value of N_{Pr} for air tabulated in ref. 21 being used). The T-prime equation used was that given by Monaghan in reference 22:

$$\frac{T_\infty'}{T_\infty} = \frac{T_w}{T_\infty} + 0.468N_{Pr}^{1/3}\left(\frac{T_r}{T_\infty} - \frac{T_w}{T_\infty}\right) - 0.273N_{Pr}\frac{\gamma - 1}{2}M_\infty^2 \tag{26}$$

In general, because N_{Pr} is evaluated at the temperature T-prime, equation (26) is solved by iteration. However, it is interesting to note that for very high Mach numbers equation (26) reduces (for N_{Pr} = Constant) to

$$\frac{T'}{T_0} = \frac{T_w}{T_0}\left(1 - 0.468N_{Pr}^{1/3}\right) + 0.468N_{Pr}^{5/6} - 0.273N_{Pr} \tag{27}$$

Therefore, for given wall and stagnation temperatures, the T-prime temperature is constant. If the value of N_{Pr} is assumed to be 0.72, equation (27) becomes

$$\frac{T'}{T_0} = 0.160 + 0.580 \frac{T_w}{T_0} \tag{28}$$

If equation (25) is assumed to apply when the proper local conditions are utilized then the effect of blunting on a flat plate may be evaluated in a simple fashion. Assume that, for the blunt-nose flat plate, the flow over the plate has passed through a normal shock and that the flow at the edge of the boundary layer is at a constant pressure p_b. The ratio of the heat-transfer coefficient for the blunt-leading-edge plate to that for the sharp-leading-edge plate is then

$$\frac{\bar{h}_b}{\bar{h}_\infty} = \frac{\sigma_\infty}{\sigma_b} \sqrt{\frac{\mu_b'}{\mu_\infty'} \frac{T_\infty'}{T_b'} \frac{u_b}{u_\infty} \frac{p_b}{p_\infty}} \tag{29}$$

in which, to repeat, the only approximations involved are the universal application of equation (25) and constant wall pressure. The factor given by equation (29) was multiplied by the result from equation (25) to obtain the values given in figure 11 for the blunt leading edge with $dp/dx = 0$ and $p_b = p_\infty$.

The heat-transfer correlation parameter $N_{St,\infty}\sqrt{R_{\infty,x}}$ is plotted in the bottom plot of figures 11(a) and (b) as obtained from the experiments of references 16 and 17 and from the hypersonically similar boundary-layer solutions. For the heat-transfer data of reference 16 (fig. 11(a)) in the range in which a power law could be fitted to the pressure data the agreement with similarity theory is considered adequate.

The data of reference 17 were obtained on a hemisphere cylinder at a Mach number of 6.8. In figure 11(b) these data are compared to the present theory with the Mangler transformation applied (ref. 23) to account for the hemisphere-cylinder configuration. Also, in this figure is the calculation from reference 17 for the Stine and Wanlass theory (ref. 24). There is good agreement between the Mangler transformed hypersonic similarity theory and the Stine-Wanlass theory. (The Mangler transformation is included in the Stine-Wanlass theory.) The agreement of the theory with experiment is considered good.

A comparison of the new data obtained in this investigation with both zero-pressure-gradient theory, hypersonic similarity theory, and the theory of reference 25 is shown in figure 12. Note the difference between the heat-transfer parameter presented in figure 12 and that presented in figure 11; in figure 12 the parameter of figure 11 has been divided by the square root of the local pressure ratio p_w/p_∞ to account

in a simple manner for the variation of the local conditions. Only the theoretical values of the heat-transfer parameter at zero angle of attack are shown; however, there is not a large effect due to angle of attack. This can be shown by using equations (25) to (28) and (31) for the flat plate with the proper local conditions. The following values are obtained for the heat-transfer correlation parameter and recovery temperature for both sharp- and blunt-leading-edge flat plates with a constant wall pressure at $M_\infty = 6.9$, $T_0 = 1{,}140^\circ$ R, and $T_w = 560^\circ$ R:

α, deg	p_w/p_∞	Sharp leading edge		Blunt leading edge	
		$\frac{N_{St,\infty}\sqrt{R_{\infty,x}}}{\sqrt{p_w/p_\infty}}$	$\frac{T_r}{T_0}$	$\frac{N_{St,\infty}\sqrt{R_{\infty,x}}}{\sqrt{p_w/p_\infty}}$	$\frac{T_r}{T_0}$
10	4.32	0.385	0.854	0.340	0.907
0	1.000	.393	.844	.365	.879
-10	.139	.397	.838	.384	.857

On the model the fourth thermocouple from the shoulder ($x/t = 2.12$) was found to be faulty. Because of twisting of the bare thermocouple wires the effective thermocouple junction occurred below the skin inside surface. However, even though this caused the indicated heat transfer to be lower than the actual heat transfer, the data from this station were not eliminated in figure 12 because this fault should not seriously affect the correlation of the indicated heat transfer.

The values of p_w/p_∞ used with the experimental values of $N_{St,\infty}\sqrt{R_{\infty,x}}$ are the local measured values shown at the top of figure 12. The theoretical hypersonic similarity solution parameter is based on the value of n obtained by fitting a power law to the pressure data. The curve in figure 12 labeled Cohen-Reshotko was calculated using the "linear method" suggested in reference 25. The required local external flow conditions on the cylindrical nose were evaluated from pressures calculated from the modified Newtonian concept plus a Prandtl-Meyer expansion (ref. 26) and on the slab, from the curve (shown in the top plot of figure 12) for the power law fitted to the experimental pressures. In figure 12 there is good agreement between the Cohen-Reshotko theory and the hypersonic similarity theory especially considering the fact that the local Mach numbers on the plate were in the range from 2.1 to 2.6 at $\alpha = 0^\circ$ which is low for the assumption of hypersonic flow. The agreement of both theories with experiment is good except near the cylinder-slab junction and the correlation of the heat-transfer data is considered good. The range of pressures involved, in the data shown

in figure 13, is about a factor of 10; however, the utilization of the square root of local pressure ratio to account for local conditions collapses the heat-transfer parameter to nearly a single curve.

The range of heat-transfer data available has included only small to moderate pressure gradients. Thus, it has not been possible to check critically the pressure-gradient effects predicted by hypersonic similarity theory. However, it is clear that the simple correction for varying local conditions - the square root of the local pressure ratio - offers a convenient method for assessing the effect on the heat transfer of pressure gradients and angle of attack. This concept is pursued further in the next section.

EXPERIMENTAL EVIDENCE FOR EFFECT OF PRESSURE GRADIENT ON BOUNDARY-LAYER THICKNESS

Equation (6) indicates that locally high pressures will thin the boundary layer. Figure 7(a) shows that, in a favorable pressure gradient, the gradient itself has a relatively small effect on the boundary-layer thickness. Data are available for boundary-layer thicknesses on a sharp flat plate in reference 27 and a blunt flat plate in references 16 and 28. The free-stream Mach numbers for these data are in the range from 4 to 6. Because of these relatively low test Mach numbers the displacement thickness of the boundary layer and the total thickness are not the same. In addition, but also related to the low test Mach numbers, the definition of the edge of the boundary layer is arbitrary; that is, it can be defined on the basis of velocity, shear, or total-pressure profiles. Different sets of data cannot be compared because of this. However, for any set of data in a pressure gradient with a consistent definition for the edge of the boundary layer, it should be possible to obtain a check on certain of the theoretical concepts.

The data obtained on a sharp-leading-edge flat plate at a free-stream Mach number of 5.8 by Kendall (ref. 27) are shown in figure 13. For these data, the pressure variation (shown in the top plot of fig. 13) is entirely the results of the displacing effect of the boundary layer. In the center plot of figure 13 is shown the boundary-layer thickness in the form of the correlating parameter given by zero-pressure-gradient theory. Note the drop off in the boundary-layer-thickness parameter at the lowest Reynolds numbers. In the bottom plot of figure 13, the boundary-layer-thickness parameter has been modified to the form suggested by equation (6) which includes the square root of the local pressure ratio to account for variation of local conditions. The data in this form are found to be essentially independent of Reynolds number as predicted by theory.

In reference 16, Creager presents boundary-layer-thickness measurements on an unyawed hemicylinder-nose slab at zero angle of attack and a Mach number of 3.95. In this case the pressures induced on the slab are due to a combination of leading-edge bluntness and boundary-layer-displacement effects. These measured pressures are shown in the top plot of figure 14. Toward the rear of the slab the pressures drop off more rapidly than on the forward part of the slab. This behavior near the trailing edge is believed to be due to side- or trailing-edge geometry and viscous effects or a combination of both. These effects show up in the measured boundary-layer thicknesses. In the center of figure 14 again is shown the boundary-layer-thickness correlating parameter given by zero-pressure-gradient theory. The slope of this parameter as a function of distance is marked. When modified to account for local conditions by using the square root of the local pressure ratio according to hypersonic theory, the boundary-layer-thickness parameter is essentially independent of distance from the leading edge except for the stations near the trailing edge which were discussed previously.

Creager has also obtained pressure and boundary-layer-thickness measurements (ref. 28) on an unyawed hemicylinder-nose slab at a Mach number of 5.7 and angles of attack of 0° and 10°. These data are shown in figure 15. Here the pressures obtained on the slab are due to the angle of attack as well as leading-edge-bluntness and boundary-layer-displacement effects. The pressure drop off toward the trailing edge is more pronounced in this case than in his previous data (fig. 14). In fact at both angles of attack the pressures at the trailing edge drop well below the inviscid sharp-plate value, a behavior which is not expected unless there are the side and trailing edges mentioned for the previously presented data at a Mach number of 3.95. At both angles of attack, the pressures at $x/t > 10$ appear to be affected by the trailing edge. The boundary-layer-thickness correlating parameter shown in the center of figure 15 shows a considerable drop off as the leading edge is approached. When, as before, the square root of local pressure ratio is included the dependence of the boundary-layer-thickness correlating parameter on surface distance is considerably reduced (for $x/t < 10$) and the data at both angles of attack correlate.

In figures 13 to 15, data have been presented for boundary-layer thicknesses measured in pressure fields resulting from a variety of test conditions. Among these are different free-stream Mach numbers, boundary-layer-displacement effects, leading-edge-bluntness effects, and changes in angle of attack and Reynolds number per inch. In cases where trailing-edge or tip effects did not intrude, the simple boundary-layer-thickness correlating parameter including local conditions in the form suggested by hypersonic theory is essentially independent of surface distance and other conditions.

FURTHER REMARKS ON APPLICATION OF THEORY

In cases where the pressure variation with distance is such that a power-law fit is not considered valid, a deviation from the simple approach is suggested. In such cases it is possible that a step-by-step power-law approximation to the actual pressure-distribution curve will be valid in which the boundary-layer thicknesses at the junctions between steps would be matched (analogous to the method presented in ref. 29). Another more simple approach would be to assume "local similarity" - that is, use values of the exponent n to determine local values of the coefficients K (in a manner similar to the procedure given in ref. 24).

L
1
8
5

CONCLUDING REMARKS

A procedure based on the method of similar solutions has been presented by which the skin friction, heat transfer, and boundary-layer thickness in a laminar hypersonic flow with pressure gradient may be rapidly evaluated if the pressure distribution is known. This solution which at present is restricted to power-law variations of pressure with surface distance was pointed out by Li and Nagamatsu (GALCIT Memorandum No. 25) who, however, only worked out in detail the case of the strong-interaction self-induced pressure gradient by this method. The presentation herein is for a wide range of pressure gradients both favorable and adverse though the usefulness of the results for the strong adverse pressure gradients is not clear.

This theory has been compared to results from heat-transfer experiments on blunt-nose flat plates and a cylinder at free-stream Mach numbers of 4 and 6.8. These experiments included tests made at a Mach number of 6.8 over a range of angle of attack of $\pm 10^{\circ}$. By using power-law fits to the experimentally obtained pressure distributions, reasonable agreement of the experimental and theoretical heat-transfer coefficients have been obtained as well as good correlation of the experimental results over the entire range of angle of attack studied. However, the hypersonic similarity method gives essentially a correction for the effect of pressure gradient. For the available data this correction is generally smaller than the effect of local conditions, therefore, the validity of applying this method to the blunt shapes considered herein cannot be considered to have been critically checked as yet.

Because of the arbitrariness of the definition of boundary-layer thickness and the finite Mach number of the available tests, a check of hypersonic similarity theory with measured boundary-layer thicknesses is not feasible. However, the simple concept of including local

conditions through the use of the parameter (the square root of the local pressure ratio) suggested by standard hypersonic approximations gave a boundary-layer-thickness parameter essentially independent of surface distance and other conditions such as angle of attack and variable unit Reynolds number.

Langley Research Center,
National Aeronautics and Space Administration,
Langley Field, Va., February 24, 1959.

APPENDIX A

DERIVATION OF THE HYPERSONIC EQUATIONS FOR SKIN FRICTION, HEAT TRANSFER, AND BOUNDARY-LAYER THICKNESS

The following symbols are the ones used in this appendix:

a	sonic velocity
C_f	local skin-friction coefficient
C_F	average skin-friction coefficient
c_p	specific heat at constant pressure
$C_w = \frac{\mu_w t_\infty}{\mu_\infty t_w}$	
L	length of plate
m	exponent from $U_e \propto X^m$
N_{St}	Stanton number
p	static pressure
R	Reynolds number
S	enthalpy function
t	static temperature
U	velocity in incompressible plane
u	velocity in compressible plane
X	longitudinal coordinate in incompressible plane
x	longitudinal coordinate in compressible plane
y	distance normal to surface in compressible flow

β pressure-gradient parameter, $\frac{2m}{m + 1}$

γ ratio of specific heats

δ local boundary-layer thickness

$\lambda = \frac{\mu_w t_0}{\mu_0 t_w}$

μ dynamic viscosity

ν kinematic viscosity, μ/ρ

ρ mass density

τ shear stress at surface

Subscripts:

e local flow at edge of boundary layer

0 stagnation conditions

w wall conditions

∞ undisturbed free-stream conditions

The method used to obtain equations (3) to (10) in the main text is a generalization of the derivations presented by Li and Nagamatsu in reference 9. However, in the following presentation, in general, the nomenclature of Cohen and Reshotko (ref. 4) is used. According to equation (42a) of reference 4 the wall shear is

$$C_{f,w} = \frac{2\tau}{\rho_w u_e^2} = f_w'' \left[2\lambda(1 + S_w)\right] \sqrt{\frac{m + 1}{2} \frac{\nu_0}{U_e X}} \tag{A1}$$

or

$$C_{f,w}\sqrt{R_{w,x}} = f_w'' \left[2\lambda(1 + S_w)\right] \sqrt{\frac{m + 1}{2} \frac{\mu_0}{\mu_w} \frac{u_e}{U_e} \frac{\rho_w}{\rho_0} \frac{x}{X}} \tag{A2}$$

Now, with

$$\left.\begin{aligned} \rho &\propto \frac{p}{t} \\ \lambda &= \frac{\mu_w t_0}{\mu_0 t_w} \\ 1 + S_w &= \frac{t_w}{t_0} \qquad (\text{Constant } c_p) \end{aligned}\right\} \tag{A3}$$

there is obtained

$$C_{f,w}\sqrt{R_{w,x}} = 2f_w''\left[\frac{m+1}{2}\lambda\frac{a_e}{a_0}\frac{x}{X}\right]^{1/2} \tag{A4}$$

Now X is related to x according to the modified form of Stewartson's transformation presented in equation (6b) of reference 4 where

$$X = \int_0^x \lambda \frac{p_w}{p_0}\frac{a_e}{a_0}\,dx \tag{A5}$$

and $p_e = p_w$. With isentropic flow at the edge of the boundary layer

$$\frac{a_e}{a_0} = \left(\frac{p_w}{p_0}\right)^{\frac{\gamma-1}{2\gamma}} \tag{A6}$$

and the assumption that

$$\frac{p_w}{p_0} \propto x^n \tag{A7}$$

then

$$X \propto x^{\frac{n(3\gamma-1)+2\gamma}{2\gamma}} \tag{A8}$$

or

$$\frac{X}{x} = \lambda\frac{2\gamma}{n(3\gamma-1)+2\gamma}\left(\frac{p_w}{p_0}\right)^{\frac{3\gamma-1}{2\gamma}} \tag{A9}$$

If equations (A6) and (A9) are substituted into equation (A4) the following is obtained for an invariant velocity at the edge of the boundary layer (the hypersonic assumption):

$$C_{f,w}\sqrt{R_{w,x}} = 2f_w''\sqrt{\frac{m+1}{2}}\left[\frac{n(3\gamma-1)+2\gamma}{2\gamma}\right]^{1/2}\sqrt{\frac{p_w}{p_0}} \tag{A10}$$

Now, since

$$\frac{m+1}{2} = \frac{1}{2-\beta} \tag{A11}$$

and, according to the Li-Nagamatsu hypersonic transformation (consistent with the assumption of equation (A7)),

$$\beta = \frac{1-\gamma}{\gamma}\frac{n}{n+1} \tag{A12}$$

equation (A10) becomes, when the undisturbed free stream is used as a reference,

$$\frac{C_{f,\infty}\sqrt{R_{\infty,x}}}{\sqrt{C_w}} = f_w''\sqrt{2(1+n)\frac{p_w}{p_\infty}} \tag{A13}$$

The average skin-friction coefficient is given by

$$C_F = \frac{1}{L}\int_0^L C_f\,dx \tag{A14}$$

Substituting equations (A7) and (A13) into (A14) gives

$$\frac{C_{F,\infty}\sqrt{R_{\infty,L}}}{\sqrt{C_w}} = \frac{4f_w''}{\sqrt{2(1+n)}}\sqrt{\frac{p_w}{p_\infty}} \tag{A15}$$

The heat-transfer coefficient (Stanton number) may be evaluated by using the Reynolds analogy factor given by equation (45) of reference 4 where

$$\frac{2N_{St}}{C_f} = -\frac{S_w'/S_w}{f_w''} \tag{A16}$$

Thus, utilizing equation (A13) gives:

$$\frac{N_{St,\infty}\sqrt{R_{\infty,x}}}{\sqrt{C_w}} = \frac{1}{2}\left(-\frac{S_w'}{S_w}\right)\sqrt{2(1+n)\frac{p_w}{p_\infty}} \tag{A17}$$

In order to obtain the boundary-layer thickness, for the present problem, equation (35) of reference 4 may be written as

$$y = \frac{p_0 a_0}{p_w a_e} \sqrt{\frac{2}{m+1} \frac{\nu_0 X}{U_e}} \int_0^\eta \frac{t}{t_0} d\eta \tag{A18}$$

If equations (A3), (A6), (A9), (A11), and (A12) are used with the condition that the velocity is not changing at the edge of the boundary layer, equation (A18) becomes

$$\frac{\delta}{x} \sqrt{\frac{R_{\infty,x}}{C_w}} = \frac{\gamma - 1}{2} M_\infty^2 \sqrt{\frac{p_\infty}{p_w}} \frac{2}{\sqrt{2(1+n)}} \int_0^\infty \left(S + 1 - f'^2\right) d\eta \tag{A19}$$

REFERENCES

1. Falkner, V. M., and Skan, Sylvia W.: Some Approximate Solutions of the Boundary Layer Equations. R. & M. No. 1314, British A.R.C., 1930.

2. Hartree, D. R.: On an Equation Occurring in Falkner and Skan's Approximate Treatment of the Equations of the Boundary Layer. Proc. Cambridge Phil. Soc., vol. XXXIII, pt. 2, Apr. 1937, pp. 223-239.

3. Smith, A. M. O.: Improved Solutions of the Falkner and Skan Boundary Layer Equation. Rep. ES 16009 (Contract No. NOa(s) 9027), Douglas Aircraft Co., Inc., Mar. 31, 1952.

4. Cohen, Clarence B., and Reshotko, Eli: Similar Solutions for the Compressible Laminar Boundary Layer With Heat Transfer and Pressure Gradient. NACA Rep. 1293, 1956. (Supersedes NACA TN 3325.)

5. Illingworth, C. R.: Steady Flow in the Laminar Boundary-Layer of a Gas. Proc. Roy. Soc. (London), ser. A, vol. 199, no. A1059, Dec. 7, 1949, pp. 533-558.

6. Stewartson, K.: Correlated Incompressible and Compressible Boundary Layers. Proc. Roy. Soc. (London), ser. A., vol. 200, no. A1060, Dec. 22, 1949, pp. 84-100.

7. Levy, Solomon: Effect of Large Temperature Changes (Including Viscous Heating) Upon Laminar Boundary Layers With Variable Free-Stream Velocity. Jour. Aero. Sci., vol. 21, no. 7, July 1954, pp. 459-474.

8. Li, Ting-Yi, and Nagamatsu, Henry T.: Similar Solutions of Compressible Boundary-Layer Equations. Jour. Aero. Sci., vol. 22, no. 9, Sept. 1955, pp. 607-616.

9. Li, Ting-Yi, and Nagamatsu, H. T.: Hypersonic Viscous Flow on a Noninsulated Flat Plate. GALCIT Memo. No. 25 (Contract No. DA-04-495-Ord-19), Apr. 1, 1955. (Also available as Res. Ser. No. 128, Purdue Engineering Experiment Station, pp. 273-287.)

10. Bertram, Mitchel H., and Henderson, Arthur, Jr.: Effects of Boundary-Layer Displacement and Leading-Edge Bluntness on Pressure Distribution, Skin Friction, and Heat Transfer of Bodies at Hypersonic Speeds. NACA TN 4301, 1958.

11. Lees, Lester: On the Boundary-Layer Equations in Hypersonic Flow and Their Approximate Solutions. Jour. Aero. Sci., vol. 20, no. 2, Feb. 1953, pp. 143-145.

12. Bertram, Mitchel H.: Boundary-Layer Displacement Effects in Air at Mach Numbers of 6.8 and 9.6. NACA TN 4133, 1958.

13. Lees, Lester, and Probstein, Ronald F.: Hypersonic Viscous Flow Over a Flat Plate. Rep. No. 195 (Contract AF 33(038)-250), Aero. Eng. Lab., Princeton Univ., Apr. 20, 1952.

14. Lees, Lester: Hypersonic Flow. Fifth International Aeronautical Conference (Los Angeles, Calif., June 20-23, 1955), Inst. Aero. Sci., Inc., 1955, pp. 241-276.

15. Bertram, M. H., and Baradell, D. L.: A Note on the Sonic-Wedge Leading-Edge Approximation in Hypersonic Flow. Jour. Aero. Sci. (Readers' Forum), vol. 24, no. 8, Aug. 1957, pp. 627-628.

16. Creager, Marcus O.: Effects of Leading-Edge Blunting on the Local Heat Transfer and Pressure Distributions Over Flat Plates in Supersonic Flow. NACA TN 4142, 1957.

17. Crawford, Davis H., and McCauley, William D.: Investigation of the Laminar Aerodynamic Heat-Transfer Characteristics of a Hemisphere-Cylinder in the Langley 11-Inch Hypersonic Tunnel at a Mach Number of 6.8. NACA Rep. 1323, 1957. (Supersedes NACA TN 3706.)

18. Bertram, Mitchel H.: Exploratory Investigation of Boundary-Layer Transition on a Hollow Cylinder at a Mach Number of 6.9. NACA Rep. 1313, 1957. (Supersedes NACA TN 3546.)

19. McLellan, Charles H., Williams, Thomas W., and Bertram, Mitchel H.: Investigation of a Two-Step Nozzle in the Langley 11-Inch Hypersonic Tunnel. NACA TN 2171, 1950.

20. O'Sullivan, William J., Jr.: Some Thermal and Mechanical Properties of Inconel at High Temperatures for Use in Aerodynamic Heating Research. Proc. A.S.T.M., vol. 55, 1955, pp. 757-763.

21. Hilsenrath, Joseph, Beckett, Charles W., et al.: Tables of Thermal Properties of Gases. NBS Cir. 564, U. S. Dept. Commerce, 1955.

22. Monaghan, R. J.: An Approximate Solution of the Compressible Laminar Boundary Layer on a Flat Plate. R. & M. No. 2760, British A.R.C., 1953.

23. Mangler, W.: Boundary Layers With Symmetrical Airflow About Bodies of Revolution. Rep. No. R-30-18, pt. 20, Goodyear Aircraft Corp., Mar. 6, 1946.

24. Stine, Howard A., and Wanlass, Kent: Theoretical and Experimental Investigation of Aerodynamic-Heating and Isothermal Heat-Transfer Parameters on a Hemispherical Nose With Laminar Boundary Layer at Supersonic Mach Numbers. NACA TN 3344, 1954.

25. Cohen, Clarence B., and Reshotko, Eli: The Compressible Laminar Boundary Layer With Heat Transfer and Arbitrary Pressure Gradient. NACA Rep. 1294, 1956. (Supersedes NACA TN 3326.)

26. Lees, Lester, and Kubota, Toshi: Inviscid Hypersonic Flow Over Blunt-Nosed Slender Bodies. Jour. Aero. Sci., vol. 24, no. 3, Mar. 1957, pp. 195-202.

27. Kendall, James M., Jr.: An Experimental Irvestigation of Leading-Edge Shock-Wave - Boundary-Layer Interaction at Mach 5.8. Jour. Aero. Sci., vol. 24, no. 1, Jan. 1957, pp. 47-56.

28. Creager, Marcus O.: The Effect of Leading-Edge Sweep and Surface Inclination on the Hypersonic Flow Field Over a Blunt Flat Plate. NASA MEMO 12-26-58A, 1959.

29. Smith, A. M. O.: Rapid Laminar Boundary-Layer Calculations by Piecewise Application of Similar Solutiors. Jour. Aero. Sci., vol. 23, no. 10, Oct. 1956, pp. 901-912.

TABLE I

SUMMARY OF PARAMETERS NEEDED FOR WALL-SHEAR, HEAT-TRANSFER, AND BOUNDARY-LAYER-THICKNESS CALCULATIONS

$S_w + 1$	β	f_w''	$-\frac{S_w'}{S_w}$	$\int_0^\infty (S + 1 - f'^2)d\eta$
2	-0.10	[a] -0.1613	[a] 0.2076	[a] 6.449
	-.1305	[a] -.0500	[a] .3139	[a] 4.713
	-.1295	[a] 0	[a] .3388	[a] 4.3839
	-.1053	[b] .120	[b] .393	[b] 3.739
	-.10	[a] .1805	[a] .4033	[a] 3.6190
	-.0202	[b] .415	[b] .460	[b] 3.029
	0	.4696	.4696	[c] 2.90316
	.30	[a] .9829	[a] .5457	[a] 2.1647
	.40	[b] 1.154	[b] .560	[b] 2.020
	.50	[a] 1.2351	[a] .5725	[a] 1.9212
	.667	[b] 1.4226	[b] .588	[b] 1.778
	1	[a] 1.7368	[a] .6154	[a] 1.5621
	1	[b] 1.7386	[b] .612	--------
	1.5	[a] 2.1402	[a] .6425	[a] 1.3495
	2.0	[a] 2.4878	[a] .6613	[a] 1.2099
1	-0.1947	[a] -0.0500	-------	[a] 3.2368
	-.198838	[a,d] 0	[a] 0.3265	[d] 2.94428
	-.195	[d] .055172	-------	[d] 2.69841
	-.19	[d] .08570	-------	[d] 2.58328
	-.18	[d] .128636	-------	[d] 2.43928
	-.16	[d] .190780	[a] .4023	[d] 2.25884
	-.14	[d] .239736	-------	[d] 2.13446
	-.10	[d] .319270	-------	[d] 1.95774
	-.05	[d] .400323	-------	[d] 1.80282
	0	.4696	.4696	[c] 1.68638
	.05	[d] .531130	-------	[d] 1.59320
	.10	[d] .587035	-------	[d] 1.51578
	.20	[d] .686708	-------	[d] 1.39239
	.286	[b] .765	[b] .520	[b] 1.322
	.30	[d] .774755	-------	[d] 1.29673
	.40	[d] .854421	[b] .526	[d] 1.21932
	.50	[d] .927680	[a] .5395	[d] 1.15482
	.60	[d] .995836	-------	[d] 1.09988
	.80	[d] 1.1202677	-------	[d] 1.01053
	1.00	[d] 1.2325877	[a] .5715	[d] .94024
	1.20	[d] 1.3357215	-------	[d] .88301
	1.60	[d] 1.5215140	[a] .5940	[d] .79443
	2.00	[d] 1.6872182	[a] .6064	[d] .72821
	2.40	[e] 1.837	-------	[e] .670

$S_w + 1$	β	f_w''	$-\frac{S_w'}{S_w}$	$\int_0^\infty (S + 1 - f'^2)d\eta$
0.6	-0.235	[a] -0.0500	[a] 0.1118	[a] 2.728
	-.246	[a] 0	[a] .3123	[a] 2.4428
	-.2483	[a] .0500	[a] .3400	[a] 2.2080
	-.24	[a] .1064	[a] .3685	[a] 1.9944
	-.20	[a] .2183	[a] .4065	[a] 1.6818
	0	.4696	.4696	[c] 1.19967
	.286	[b] .670	[b] .505	[b] .970
	.40	[b] .741	[b] .517	[b] .885
	.50	[a] .7947	[a] .5225	[a] .8300
	2.00	[a] 1.3329	[a] .5760	[a] .5178
0.2	-0.10	[a] -0.0686	[a] 0.0559	[a] 3.381
	-.2685	[a] -.0500	[a] .2286	[a] 2.392
	-.3088	[a] 0	[a] .2826	[a] 2.0326
	-.325	[a] .0493	[a] .3181	[a] 1.7914
	-.3285	[a] .0693	[a] .3305	[a] 1.7024
	-.3285	[a] .1100	[a] .3523	[a] 1.5491
	-.325	[a] .1354	[a] .3641	[a] 1.4631
	-.30	[a] .2086	[a] .3944	[a] 1.2445
	-.14	[a] .3841	[a] .4488	[a] .8522
	0	.4696	.4696	[c] .71296
	.286	--------	-------	[b] .596
	.40	--------	-------	[b] .540
	.50	[a] .6547	[a] .5038	[a] .4915
	1.50	[a] .8689	[a] .5326	[a] .3355
	2.00	[a] .9480	[a] .5414	[a] .2960
0	-0.326	[a] 0	[a] 0.2477	[a] 1.9600
	-.3657	[a] .0500	[a] .2958	[a] 1.6627
	-.3884	[a] .1400	[a] .3527	[a] 1.2886
	-.360	[a] .2448	[a] .4001	[a] .9627
	-.30	[a] .3182	[a] .4262	[a] .7720
	-.14	[a] .4166	[a] .4554	[a] .5615
	0	.4696	.4696	[c] .46960
	.286	[b] .540	[b] .409	[b] .382
	.40	[b] .561	[b] .488	[b] .351
	.50	[a] .5806	[a] .4948	[a] .3145
	2.00	[a] .7381	[a] .5203	[a] .1772

[a] Cohen and Reshotko, reference 4.

[b] Li and Nagamatsu, references 8 and 9.

[c] Equation (15).

[d] Smith, reference 3.

[e] Hartree, reference 2.

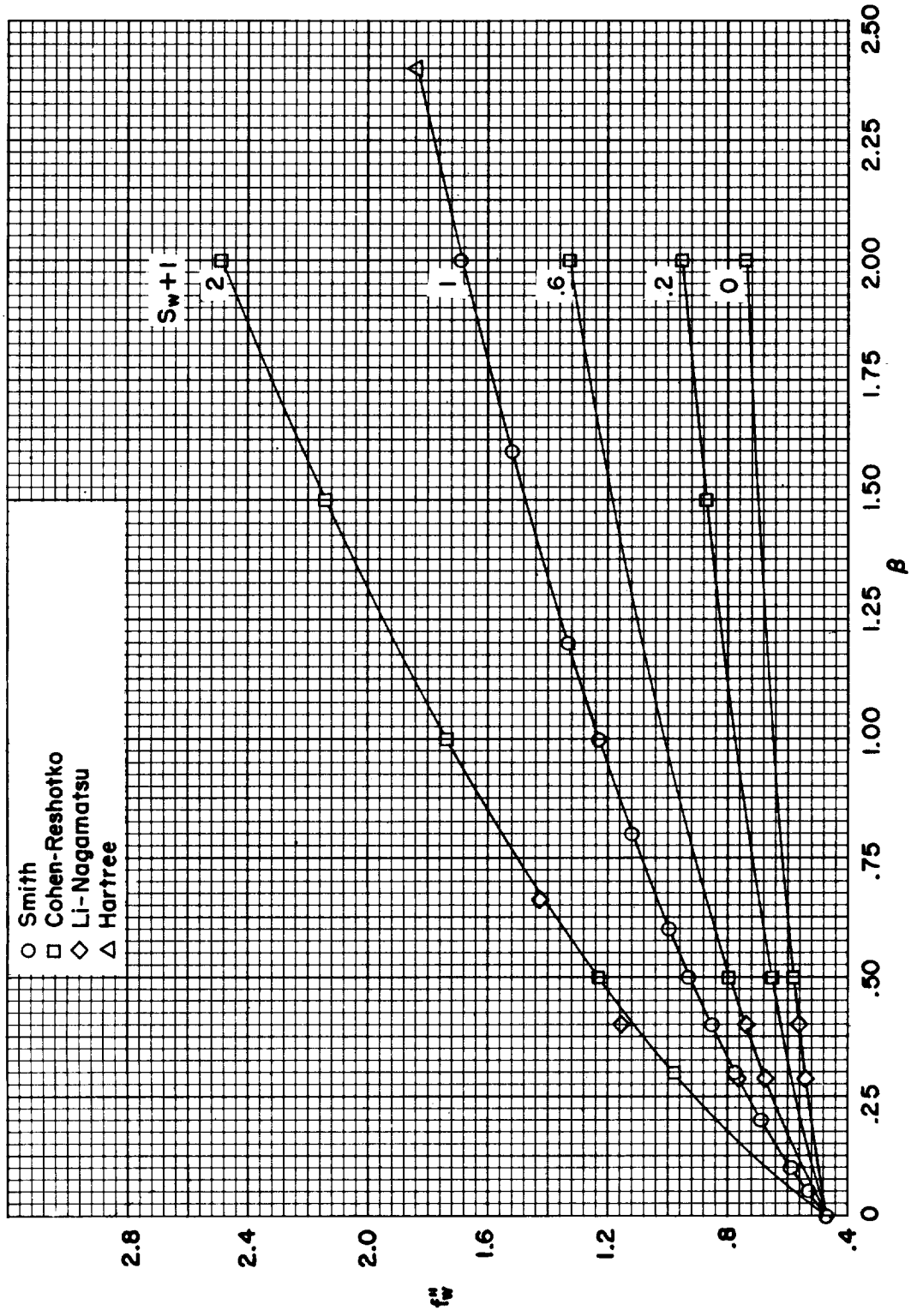

(a) Favorable pressure gradients.

Figure 1.- Variation of f_w'' with pressure gradient.

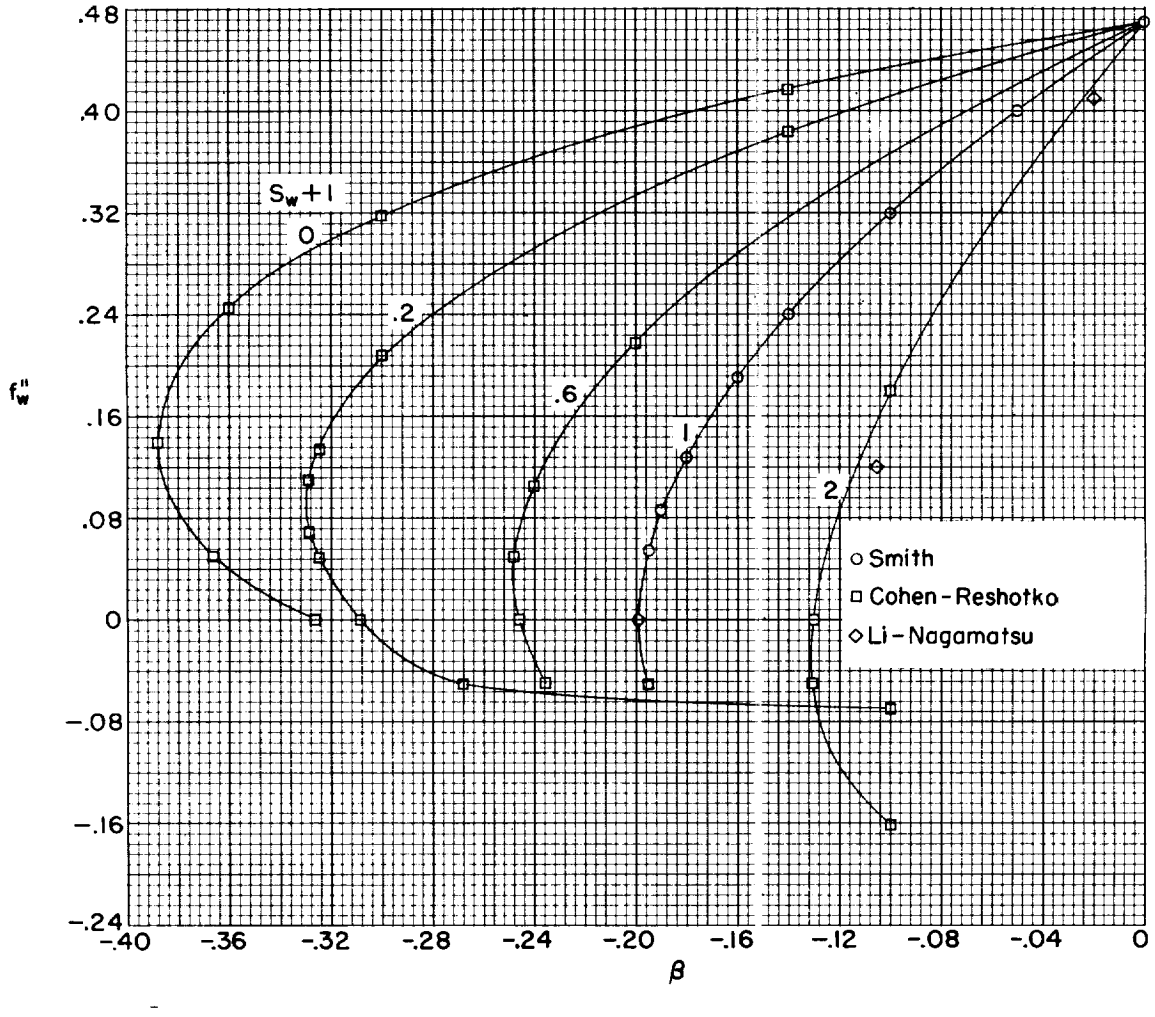

(b) Adverse pressure gradients.

Figure 1.- Concluded.

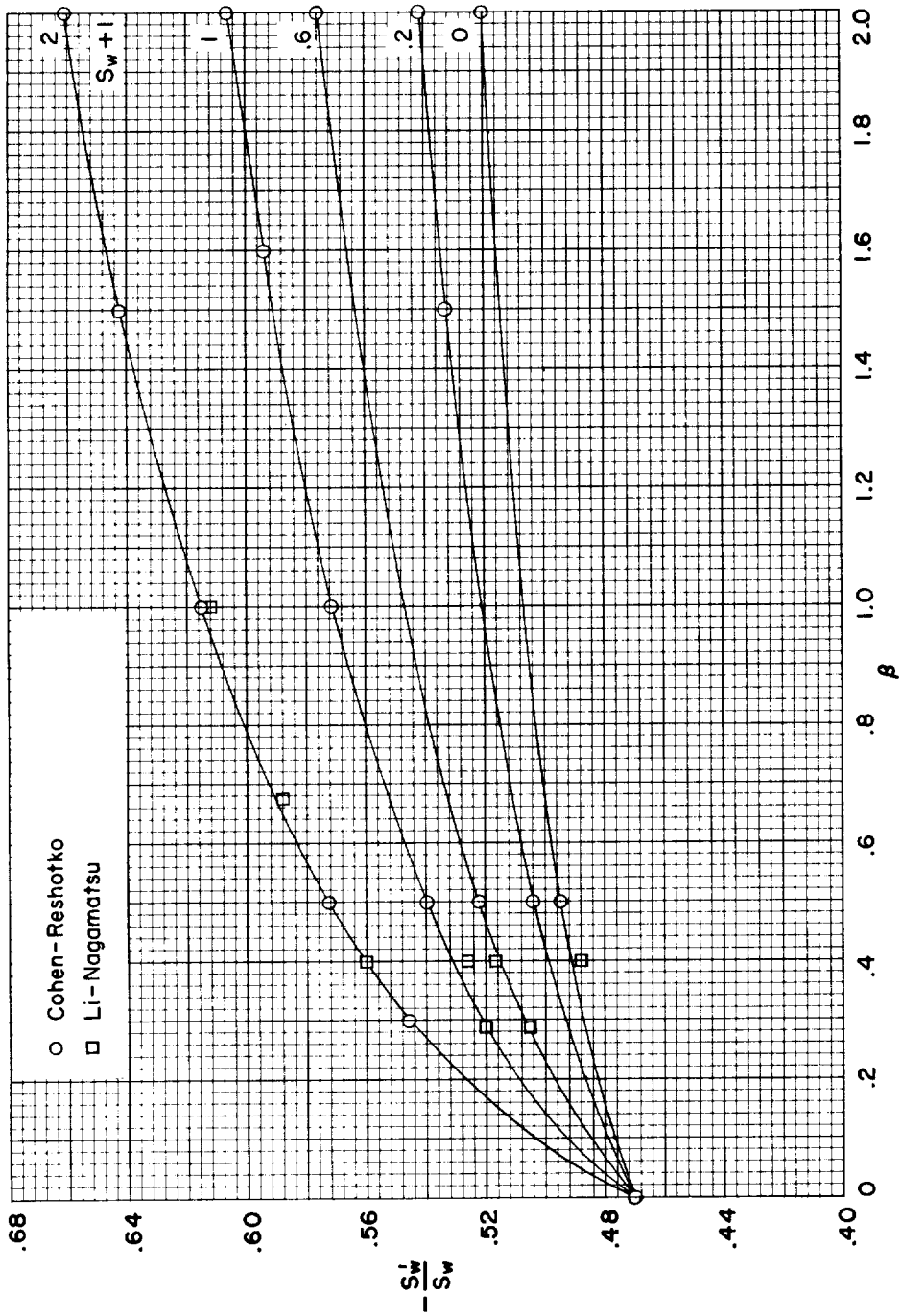

(a) Favorable pressure gradients.

Figure 2.- Variation of $\frac{S_w'}{S_w}$ with pressure gradient.

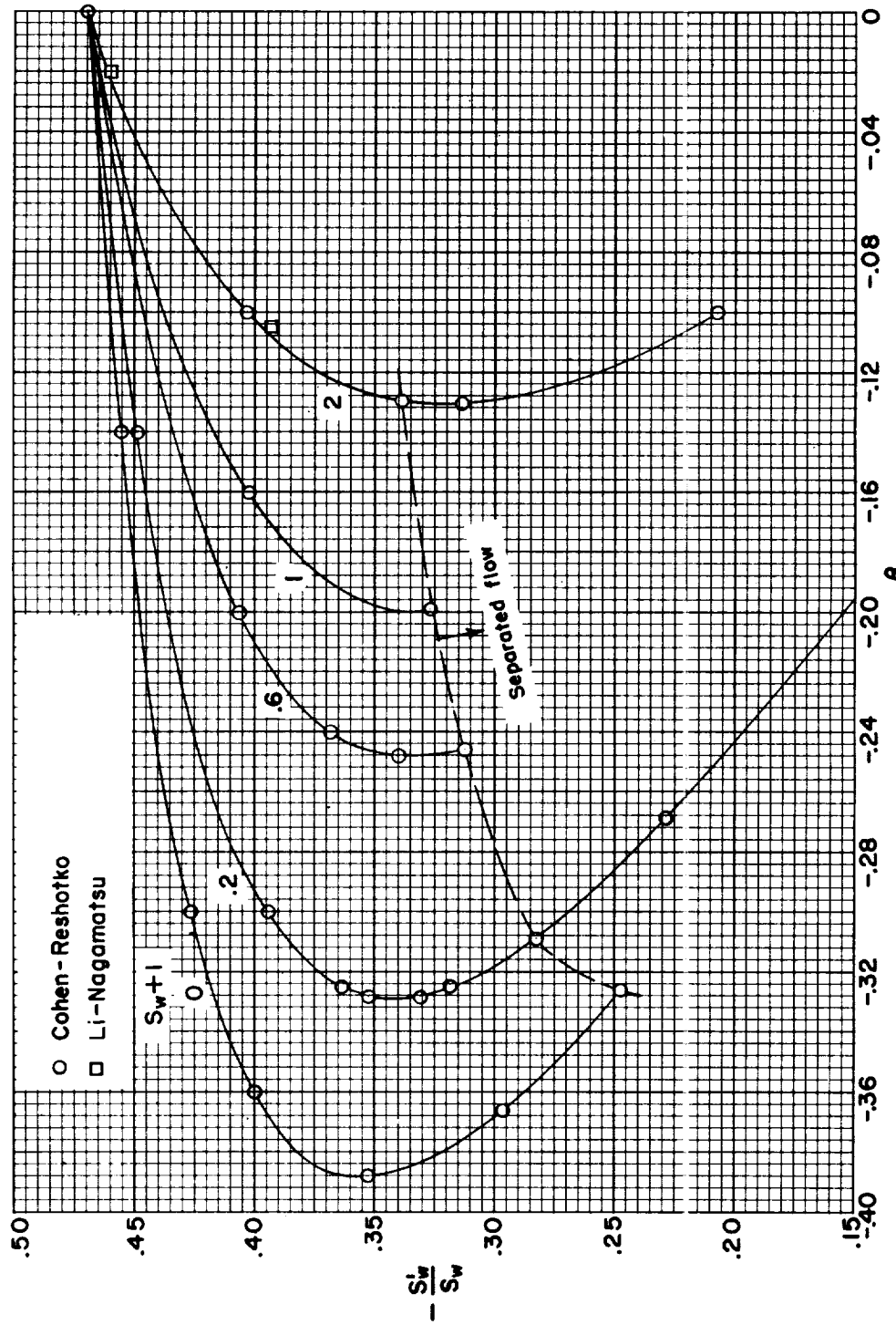

(b) Adverse pressure gradients.

Figure 2.- Concluded.

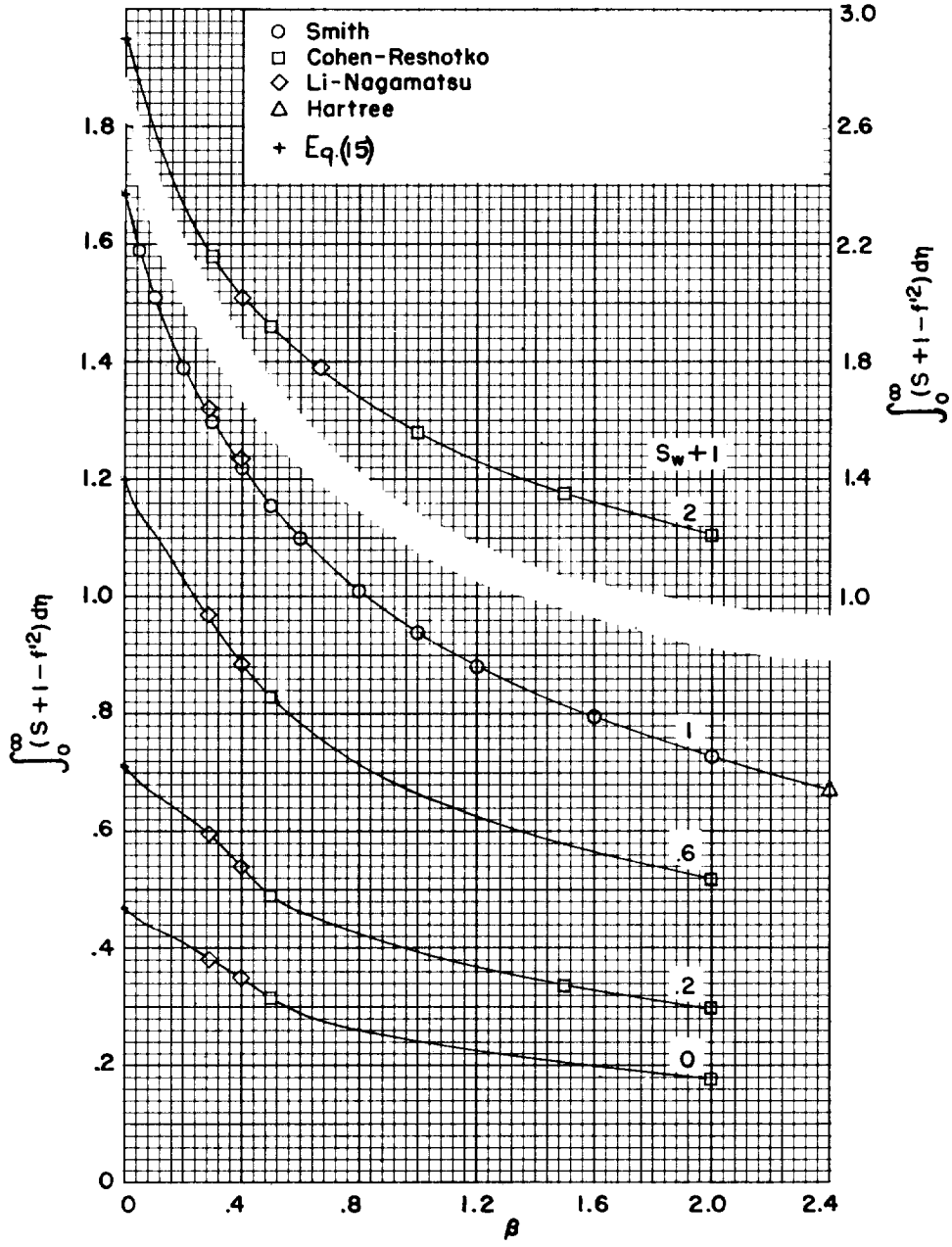

(a) Favorable pressure gradients. Note change in scale for curve for $S_w + 1 = 2$.

Figure 3.- Variation of $\int_0^\infty (S + 1 - f'^2)d\eta$ with pressure gradient.

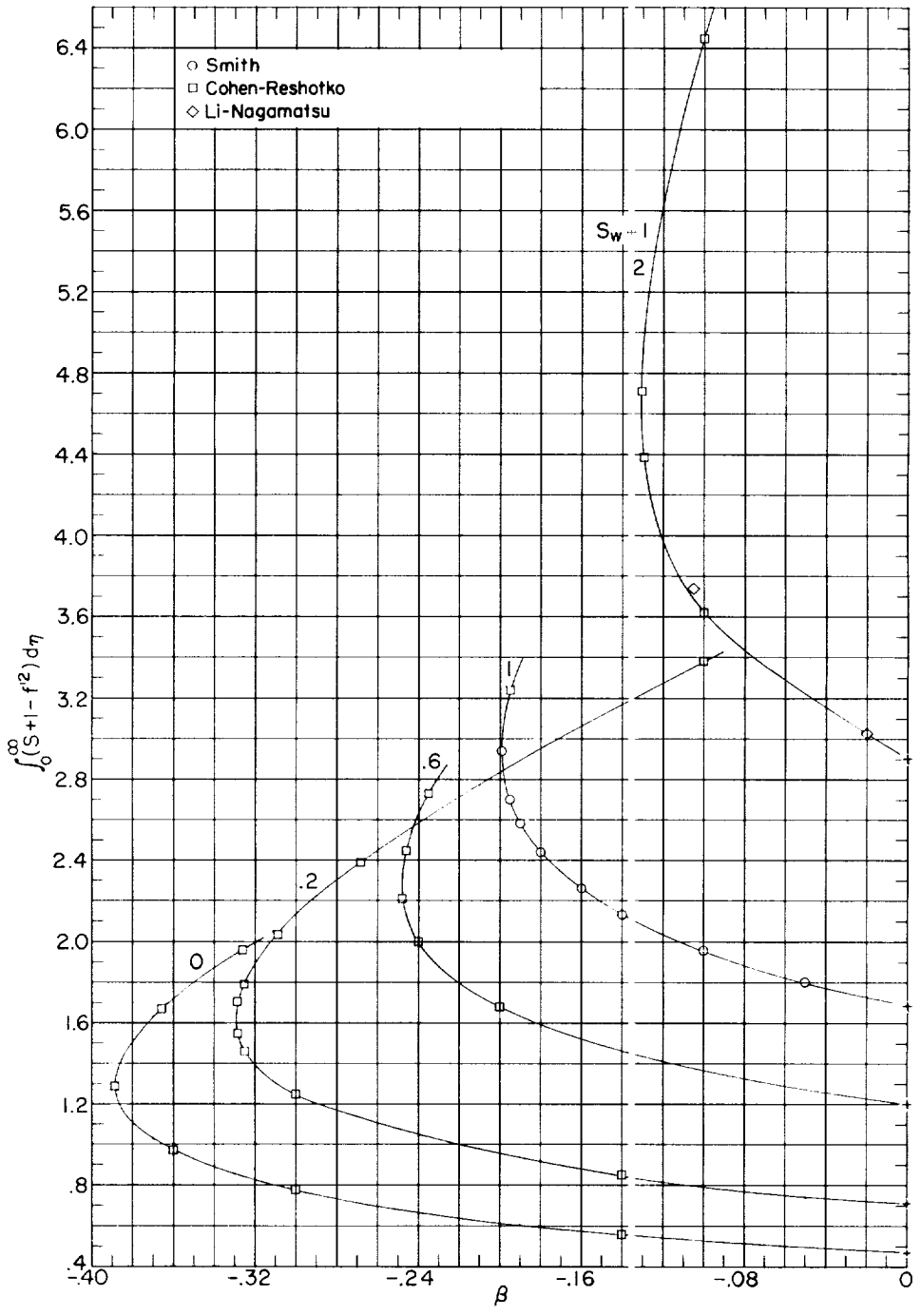

(b) Adverse pressure gradients.

Figure 3.- Concluded.

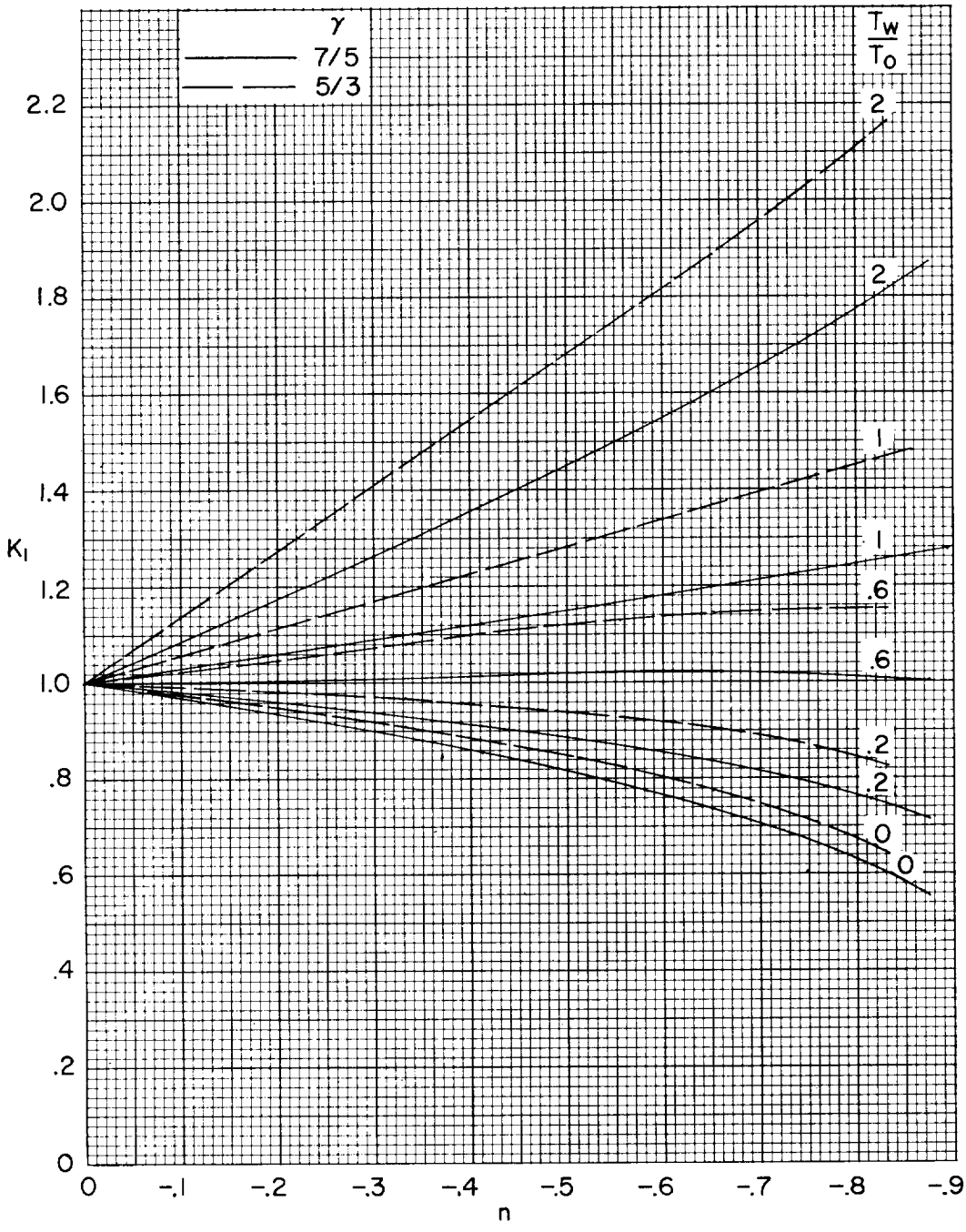

(a) Favorable pressure gradients.

Figure 4.- Variation of coefficient in local skin-friction law with pressure gradient.

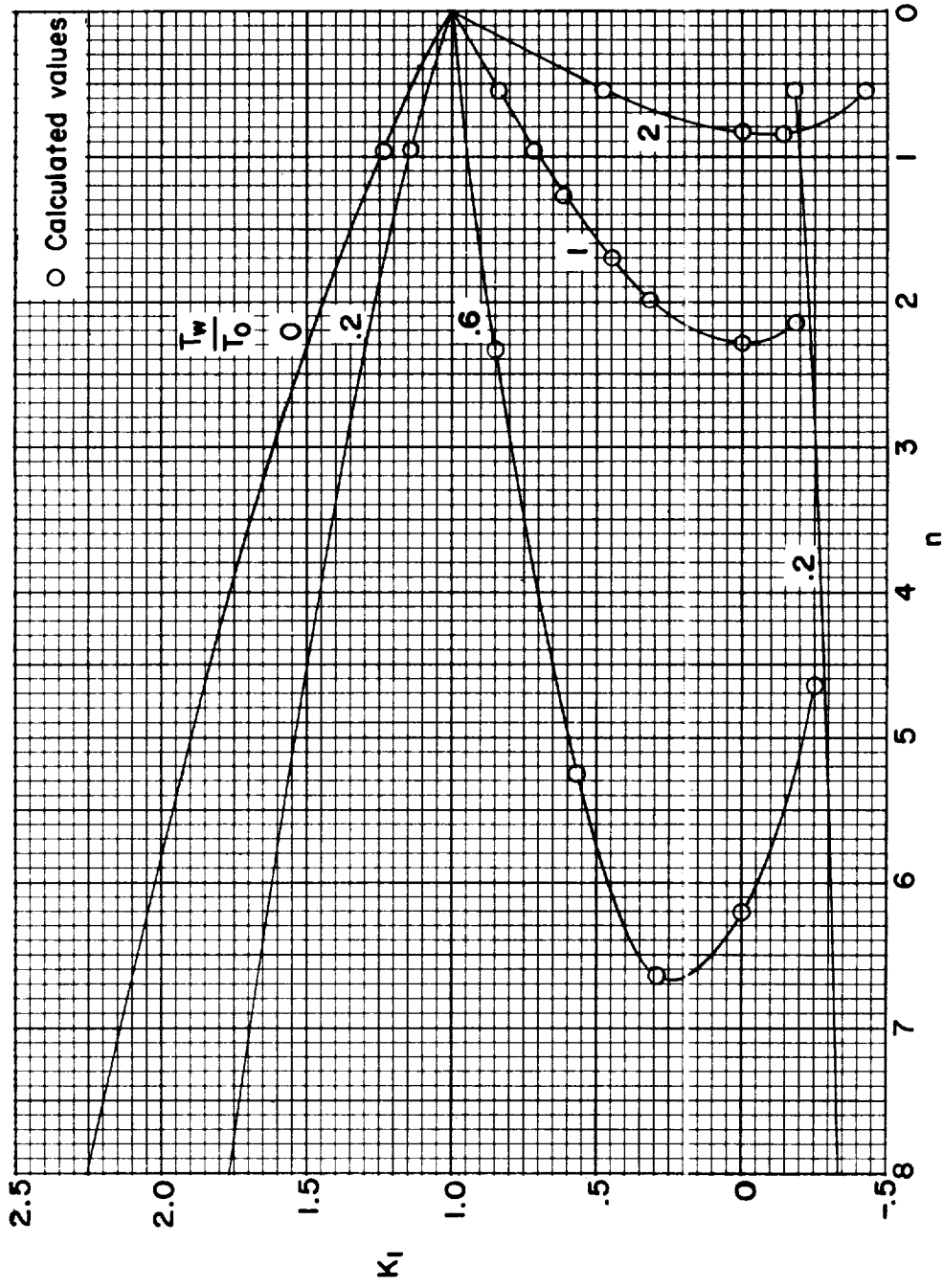

(b) Adverse pressure gradients. $\gamma = 7/5$.

Figure 4.- Continued.

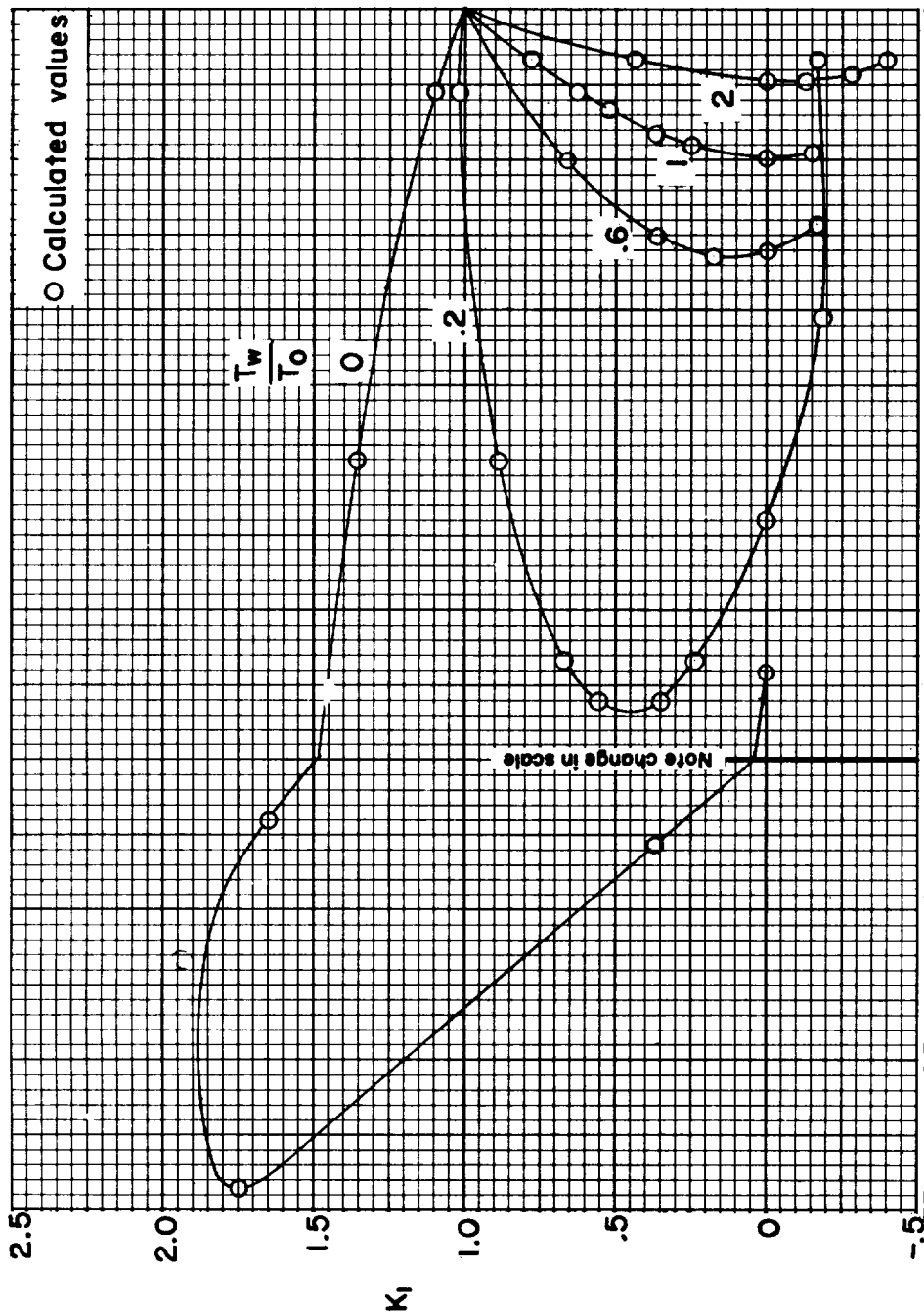

(c) Adverse pressure gradients. $\gamma = 5/3$.

Figure 4.- Concluded.

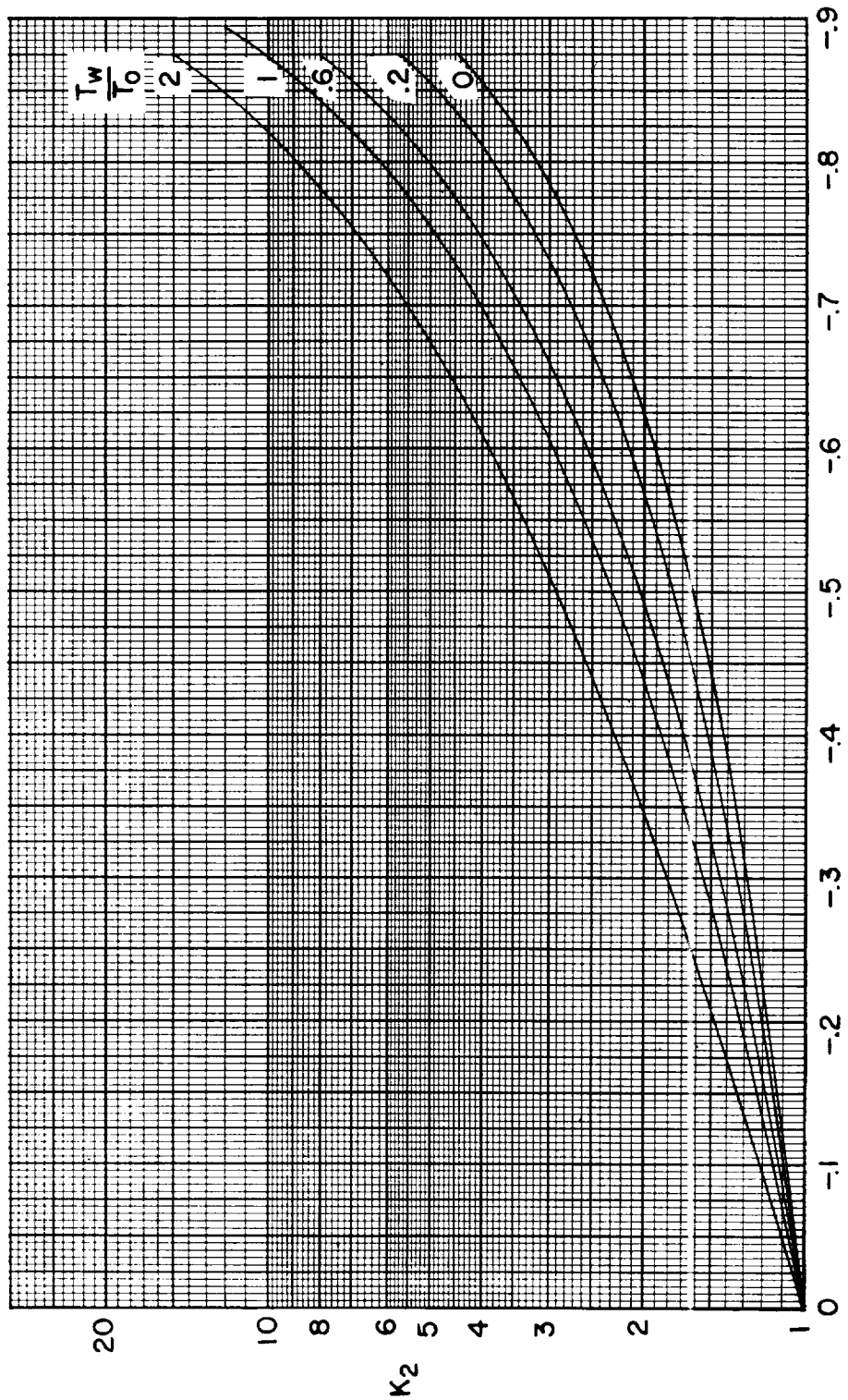

(a) Favorable pressure gradients. $\gamma = 7/5$.

Figure 5.- Variation of coefficient in average skin-friction law with pressure gradient.

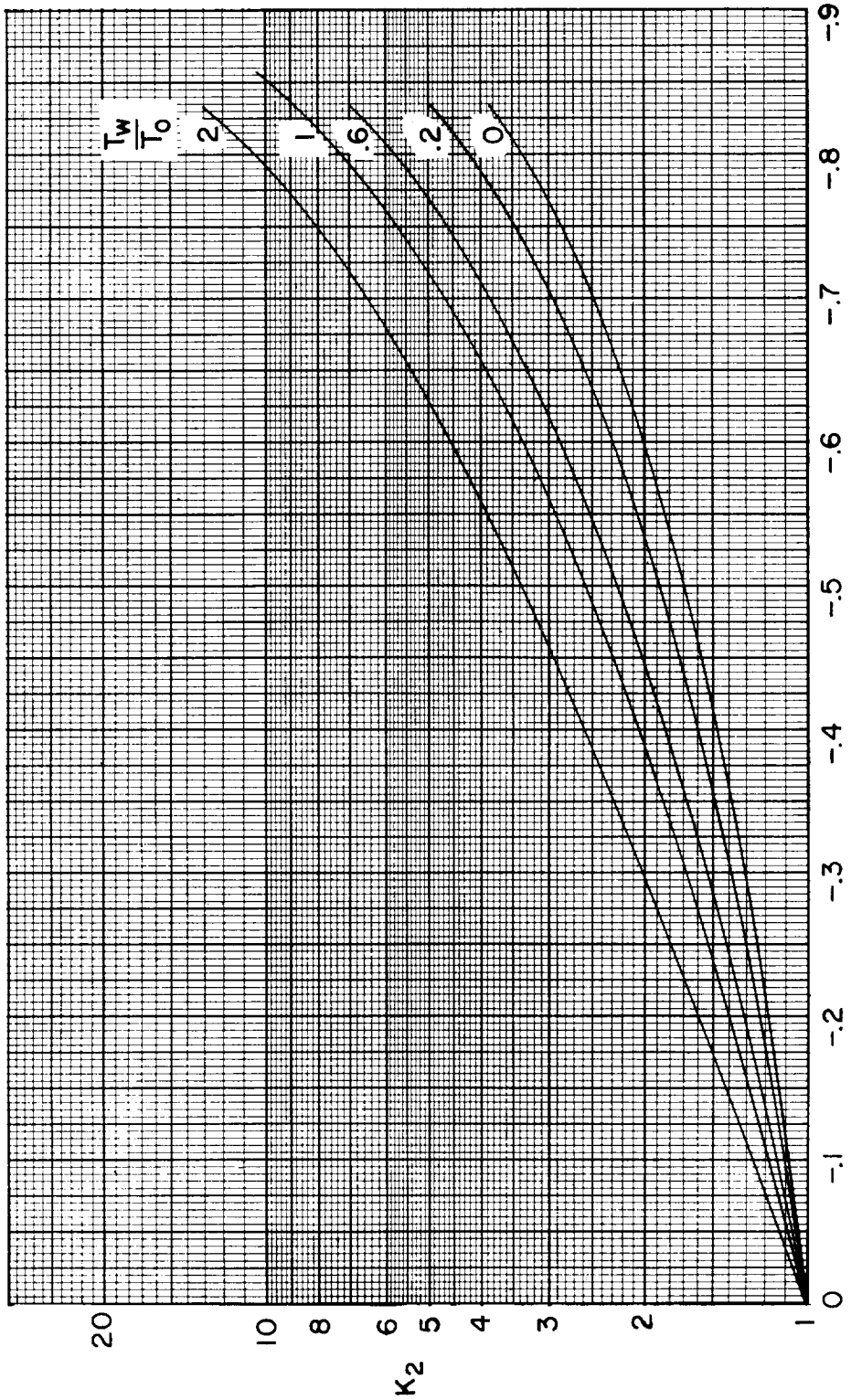

(b) Favorable pressure gradients. $\gamma = 5/3$.

Figure 5.- Continued.

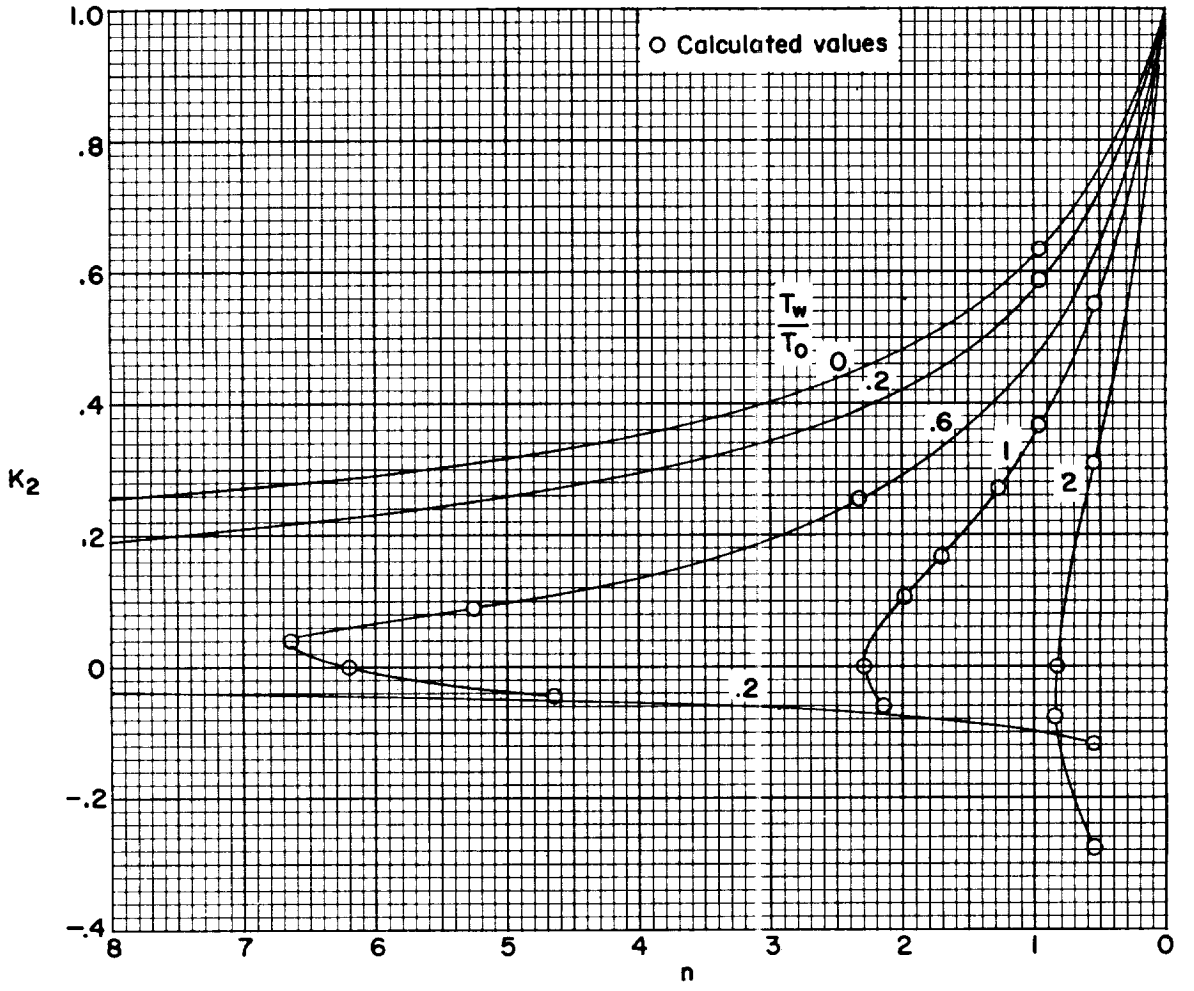

(c) Adverse pressure gradients. $\gamma = 7/5$.

Figure 5.- Continued.

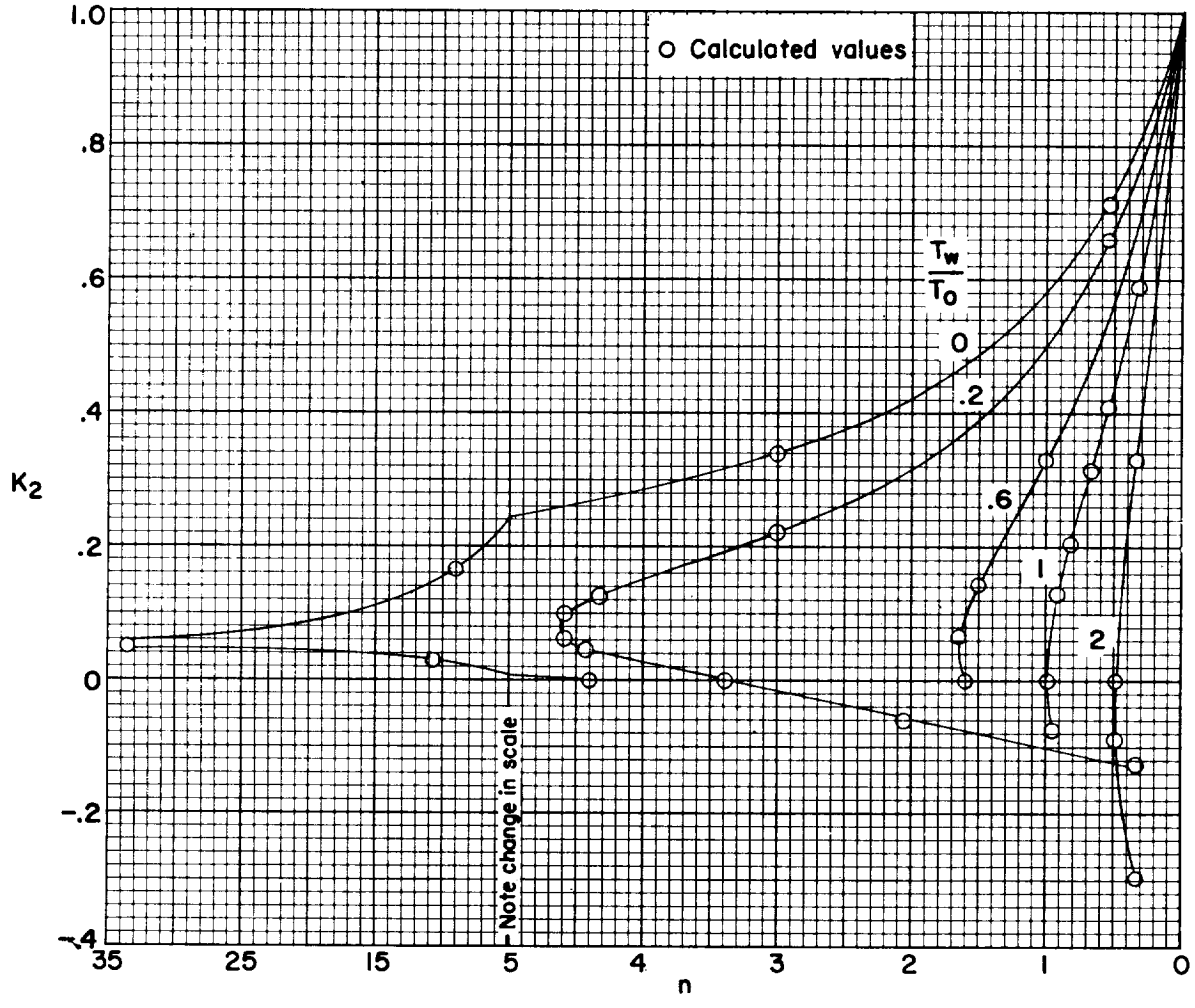

(d) Adverse pressure gradients. $\gamma = 5/3$.

Figure 5.- Concluded.

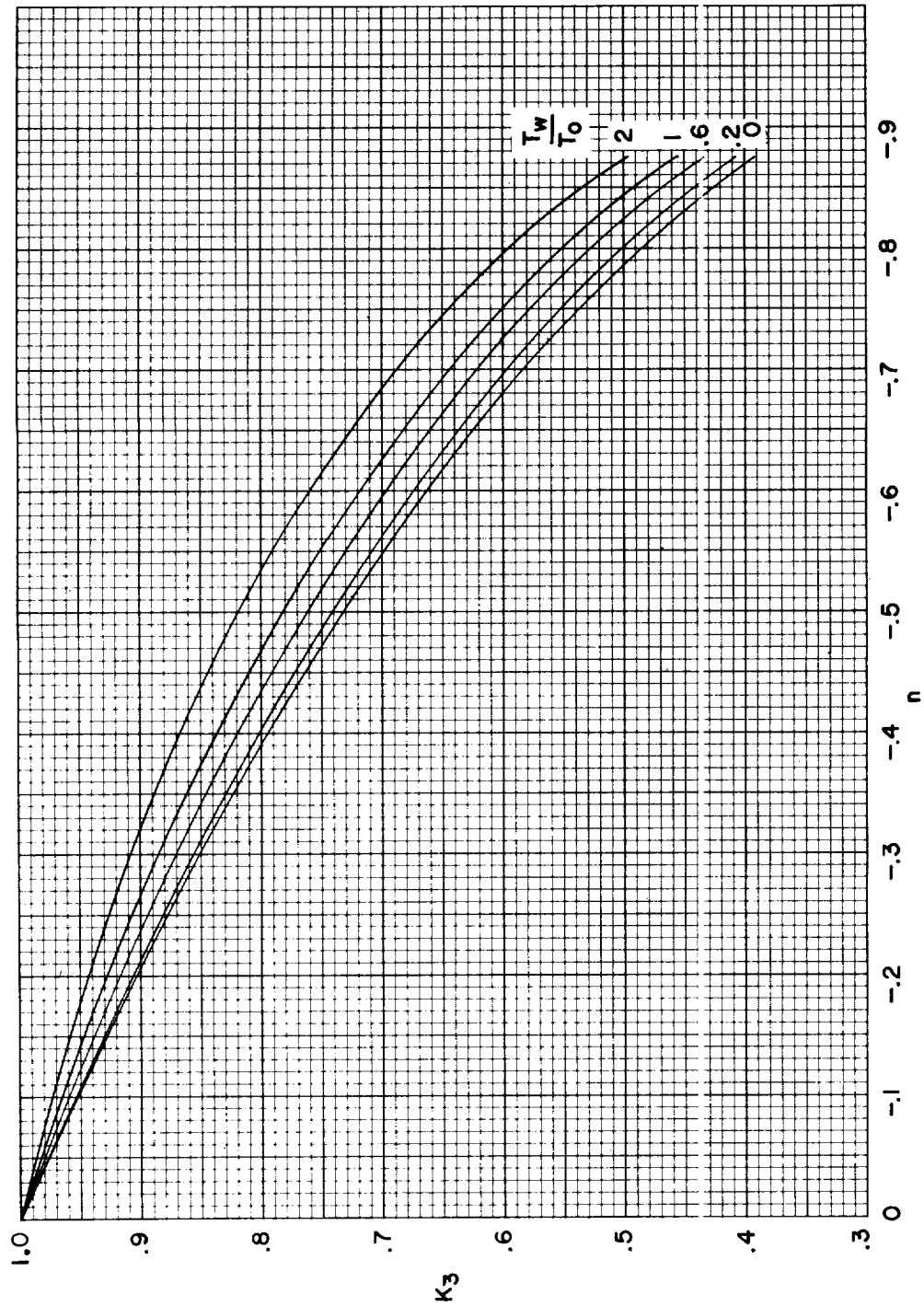

(a) Favorable pressure gradients. $\gamma = 7/5$.

Figure 6.- Variation of coefficient in heat-transfer law.

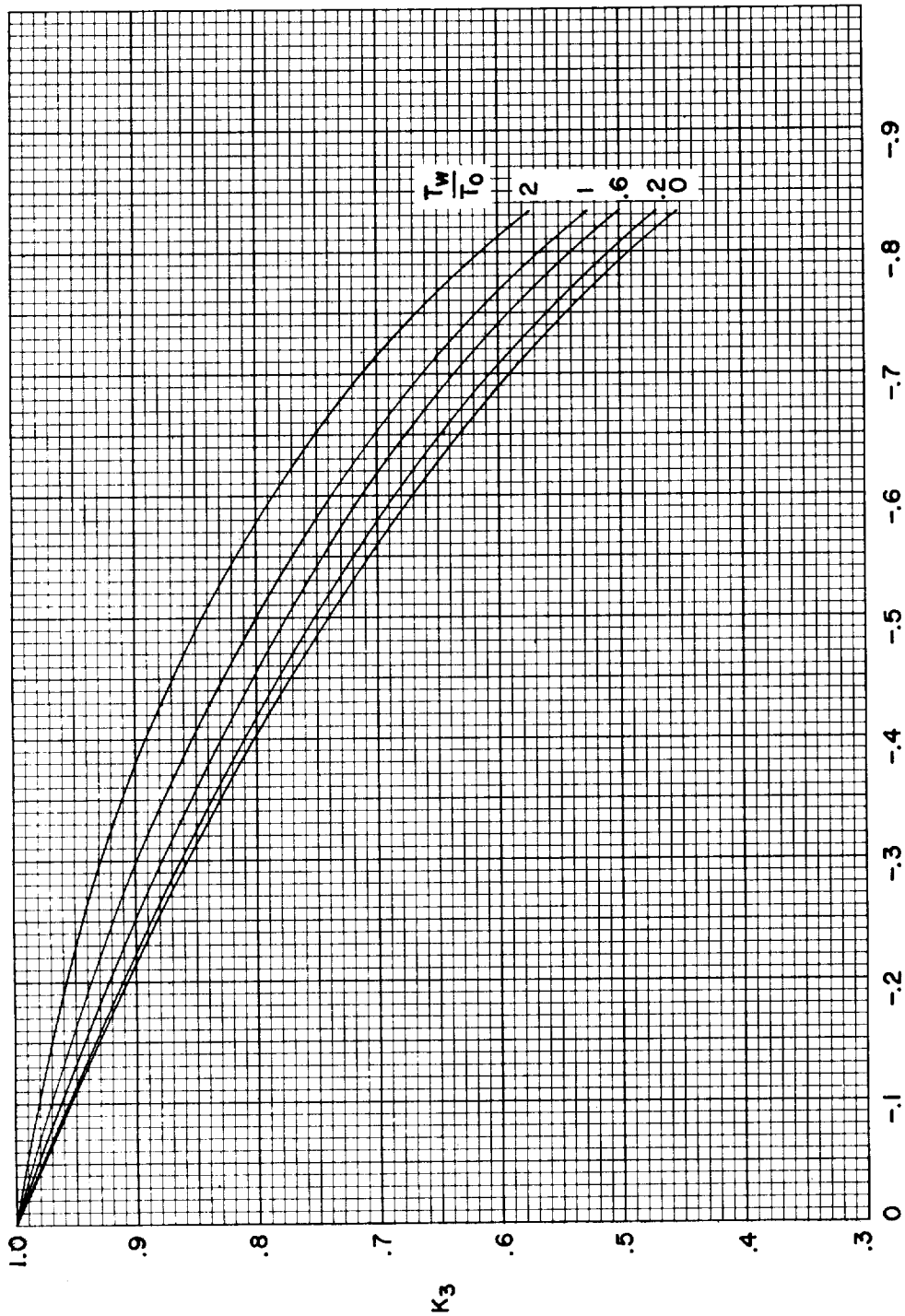

(b) Favorable pressure gradients. $\gamma = 5/3$.

Figure 6.- Continued.

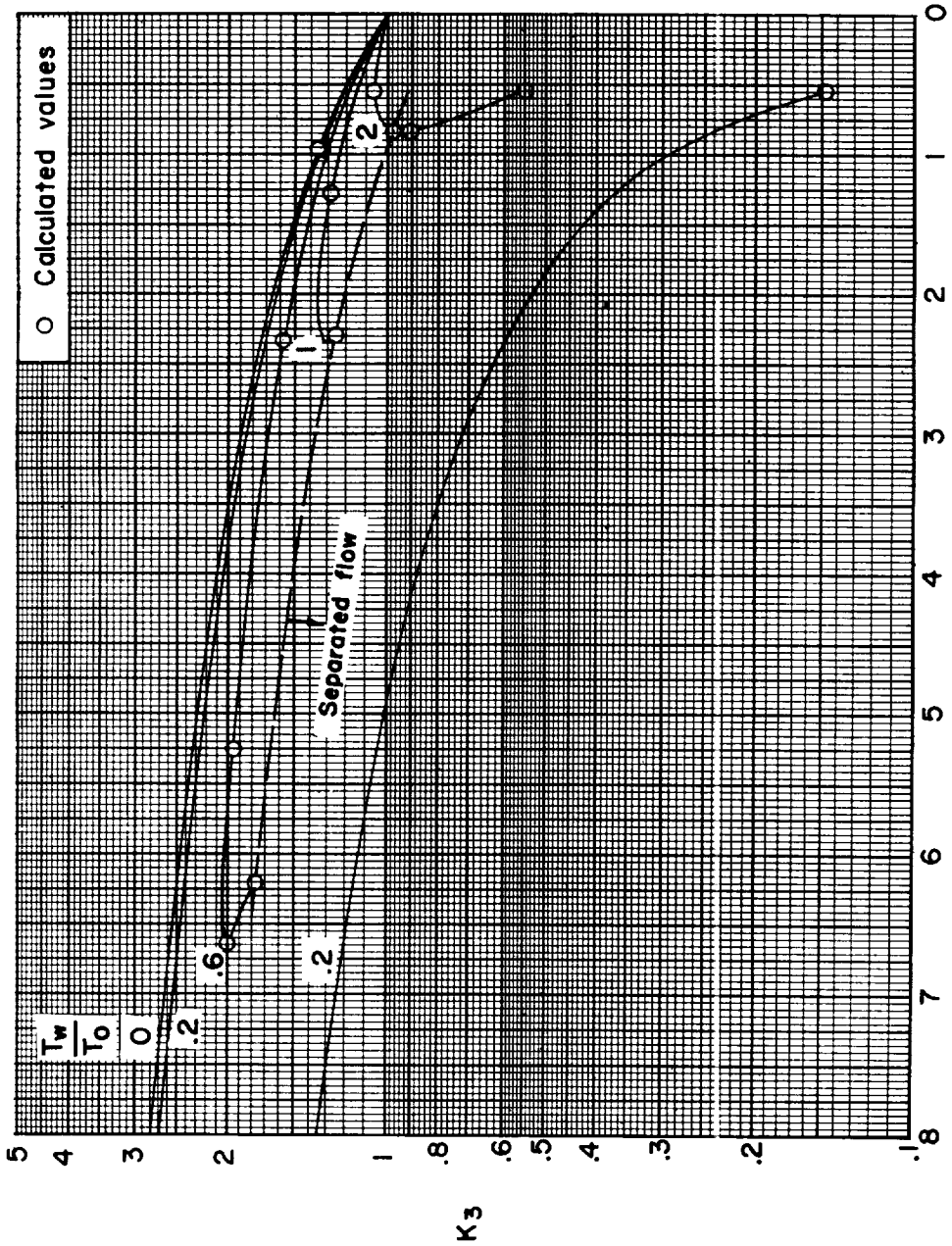

(c) Adverse pressure gradients. $\gamma = 7/5$.

Figure 6.- Continued.

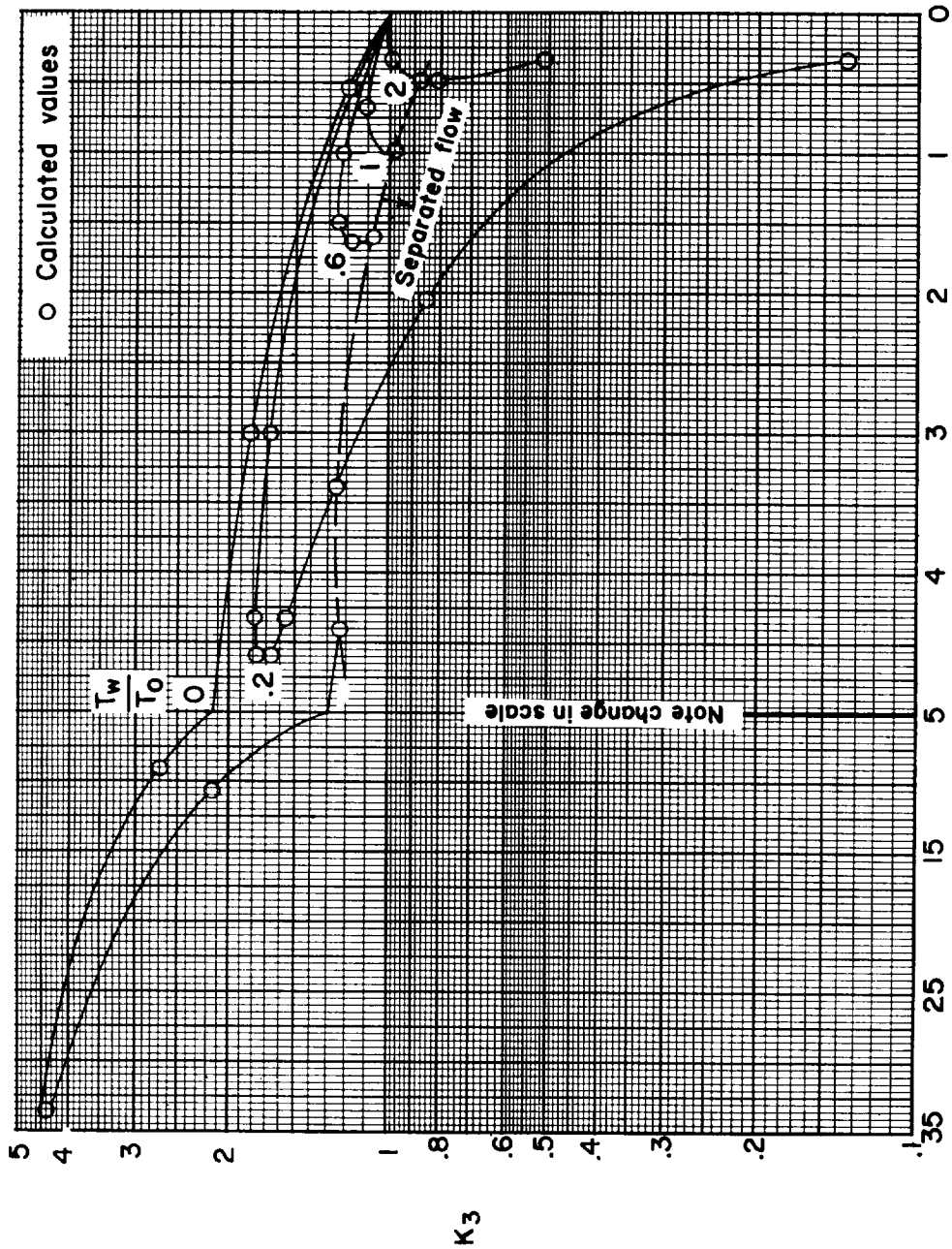

(d) Adverse pressure gradients. $\gamma = 5/3$.

Figure 6.- Concluded.

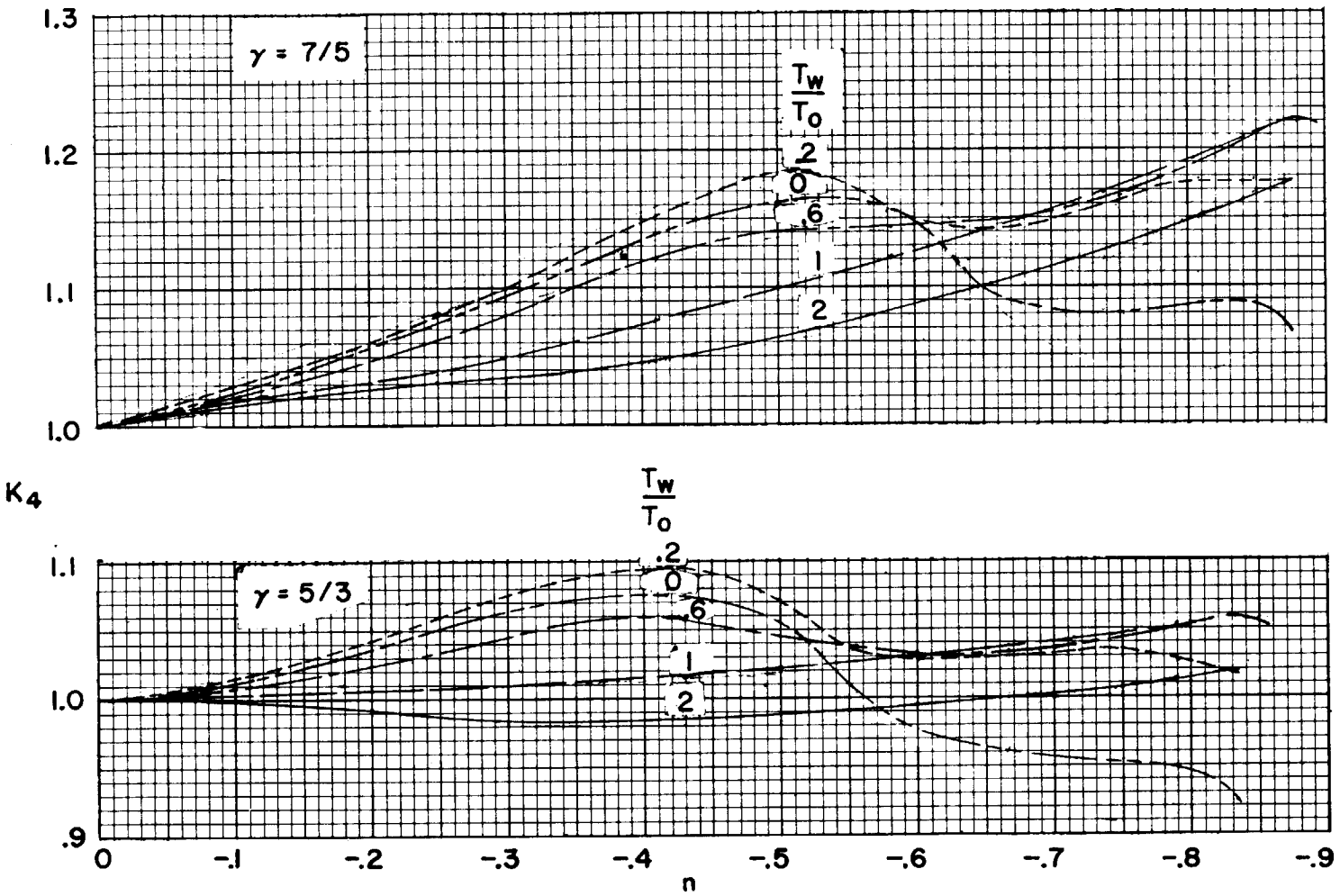

(a) Favorable pressure gradients.

Figure 7.- Variation of coefficient in boundary-layer-thickness law with pressure gradient.

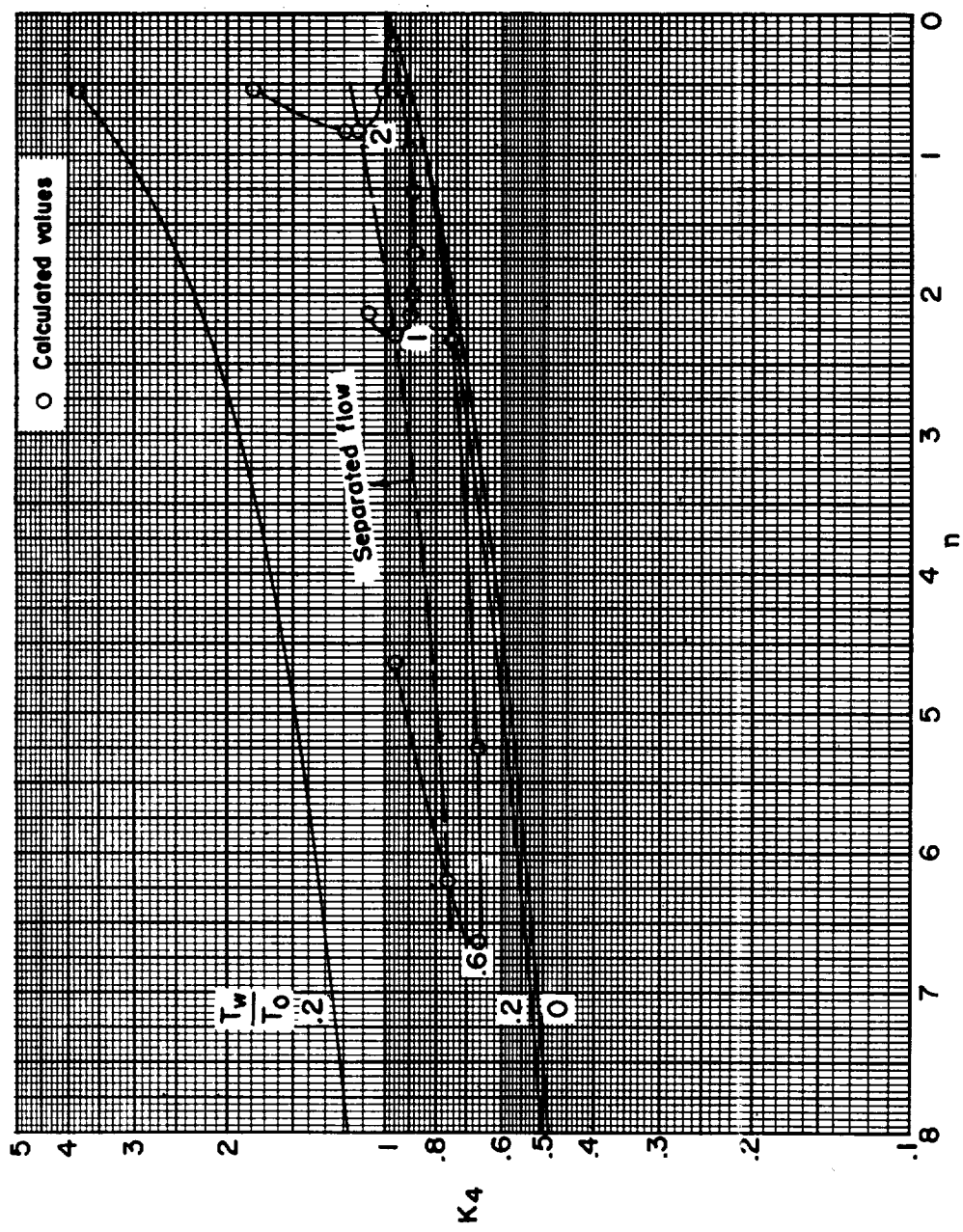

(b) Adverse pressure gradients. $\gamma = 7/5$.

Figure 7.- Continued.

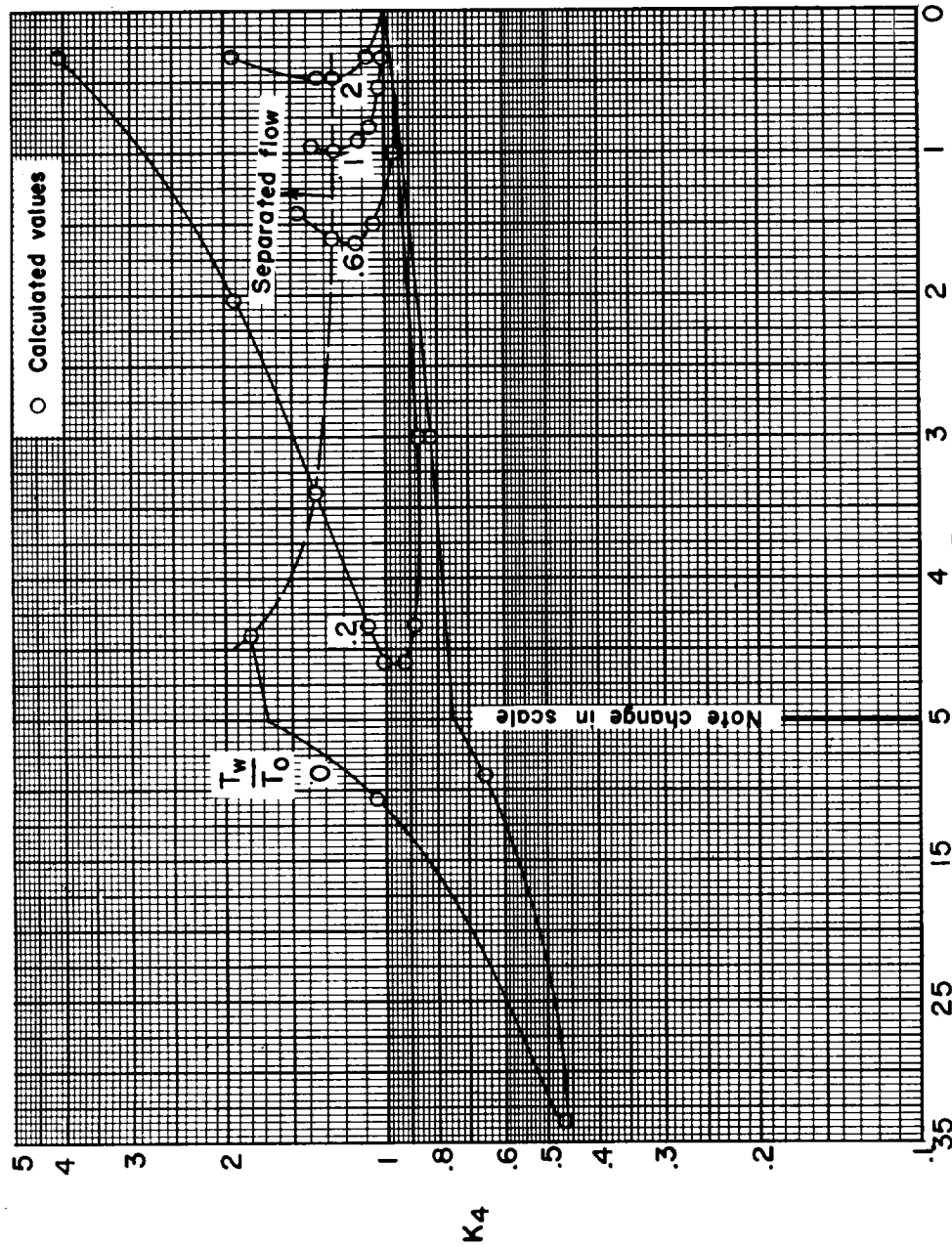

(c) Adverse pressure gradients. $\gamma = 5/3$.

Figure 7.- Concluded.

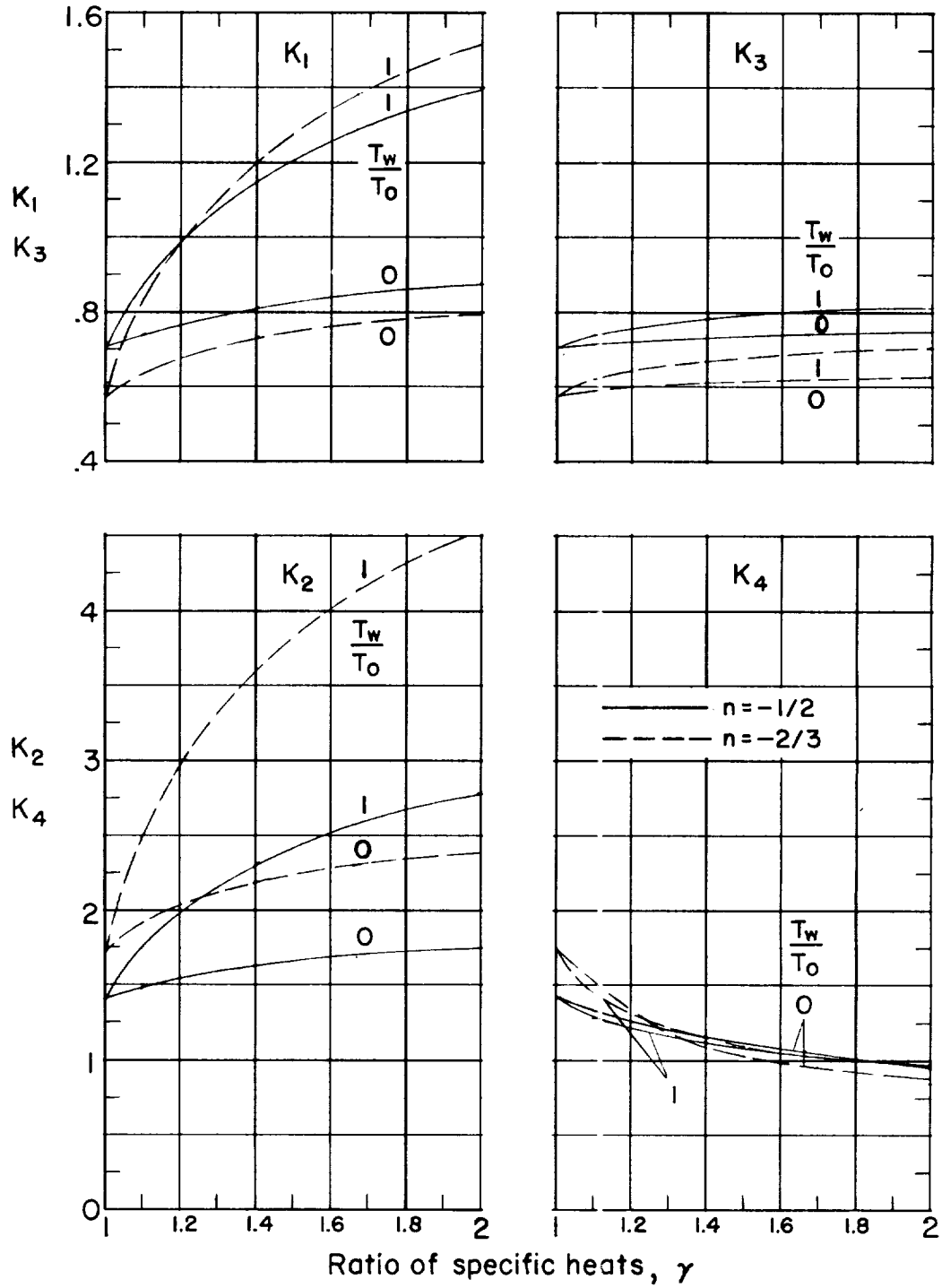

Figure 8.- Effect of γ on the coefficients K_1, K_2, K_3, and K_4.

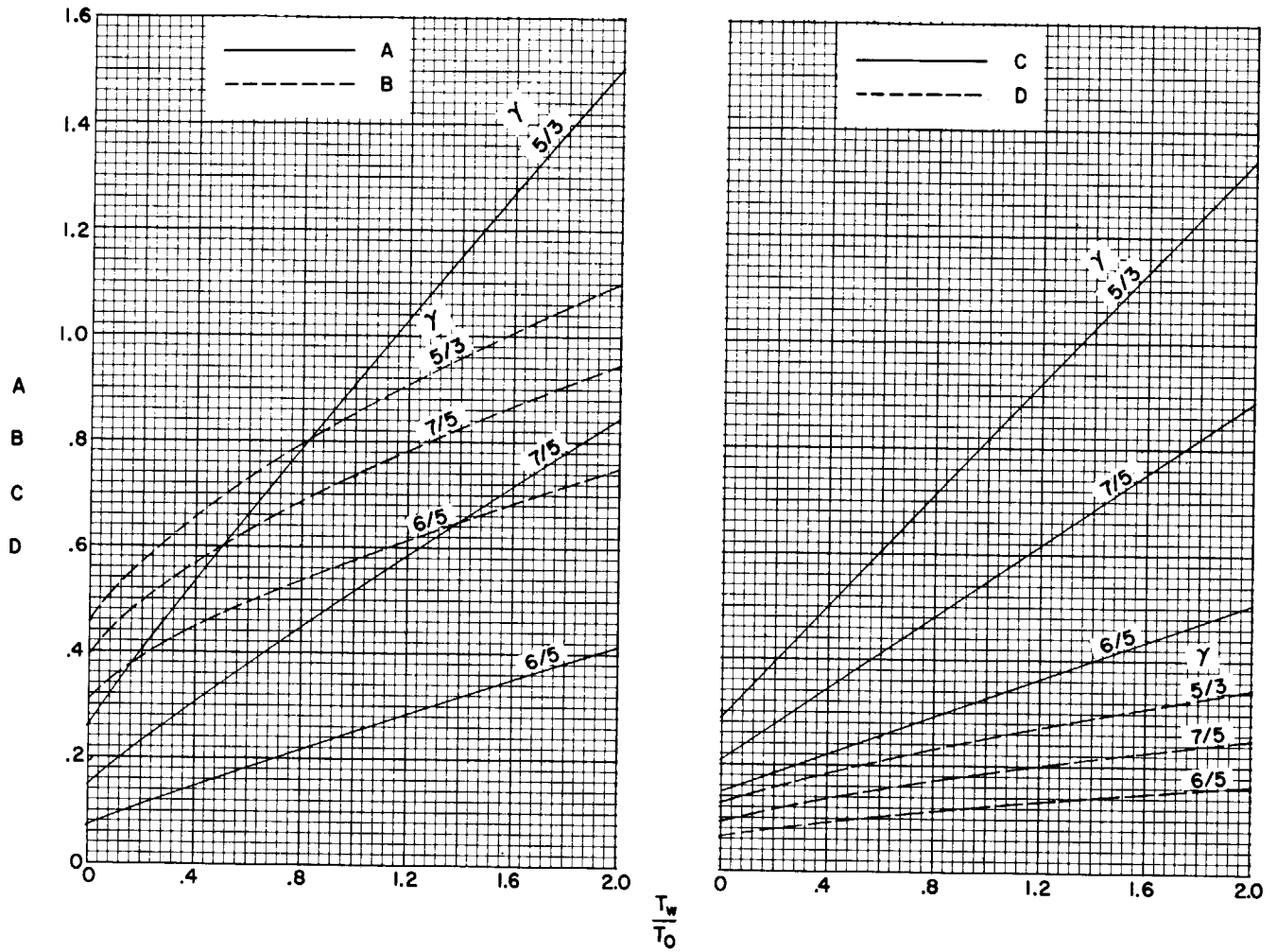

Figure 9.- Values of the coefficients in the equations for surface pressure, boundary-layer thickness, local skin friction, and heat transfer according to strong-interaction boundary-layer theory for various values of the ratio of specific heats.

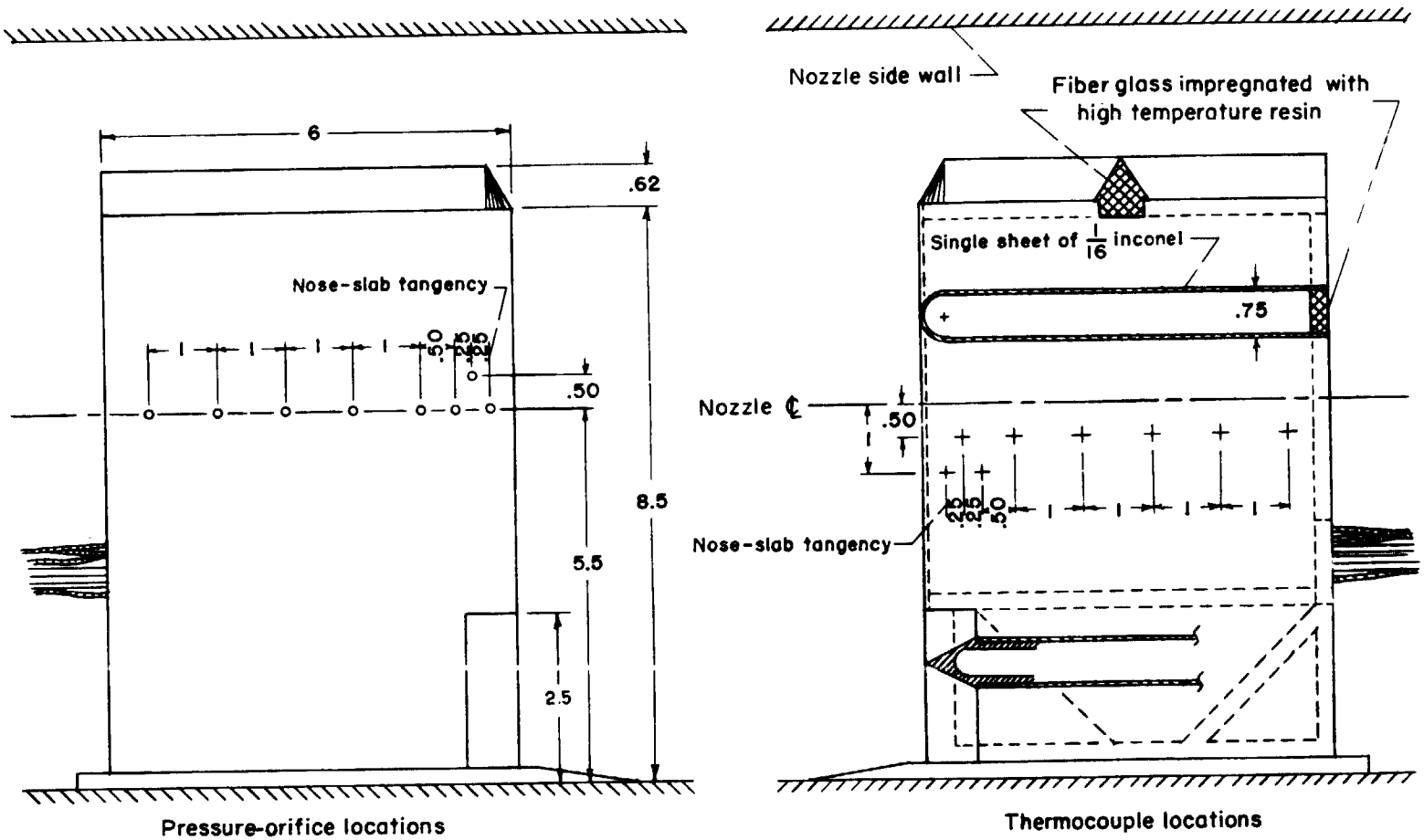

Figure 10.- Sketch of hemicylindrical-nose slab showing location of pressure orifices and thermocouples. All dimensions are in inches.

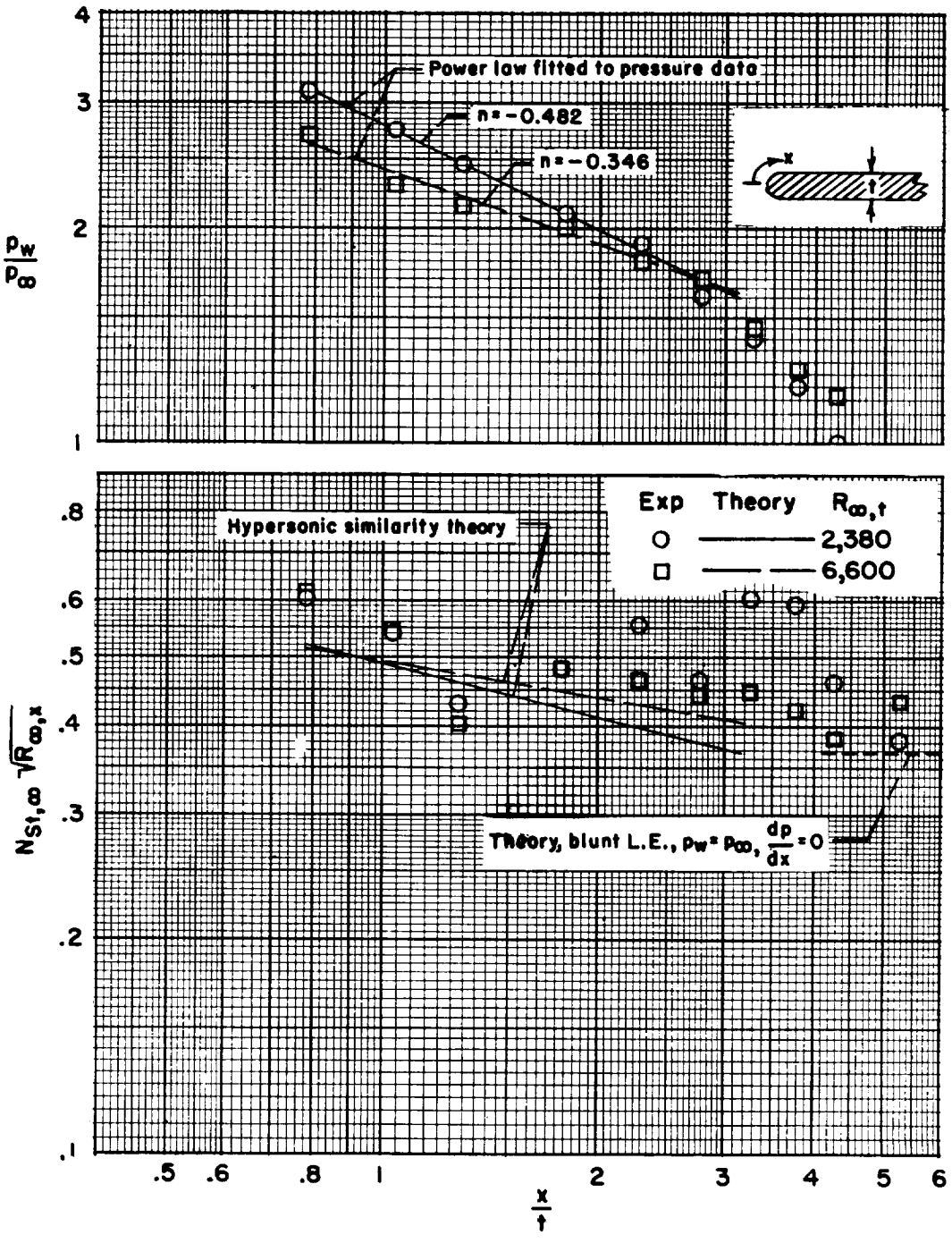

(a) Hemicylindrical-nose flat plate, reference 16. $M_\infty = 3.9$.

Figure 11.- Comparison of theory with experiment for blunt-nose bodies.

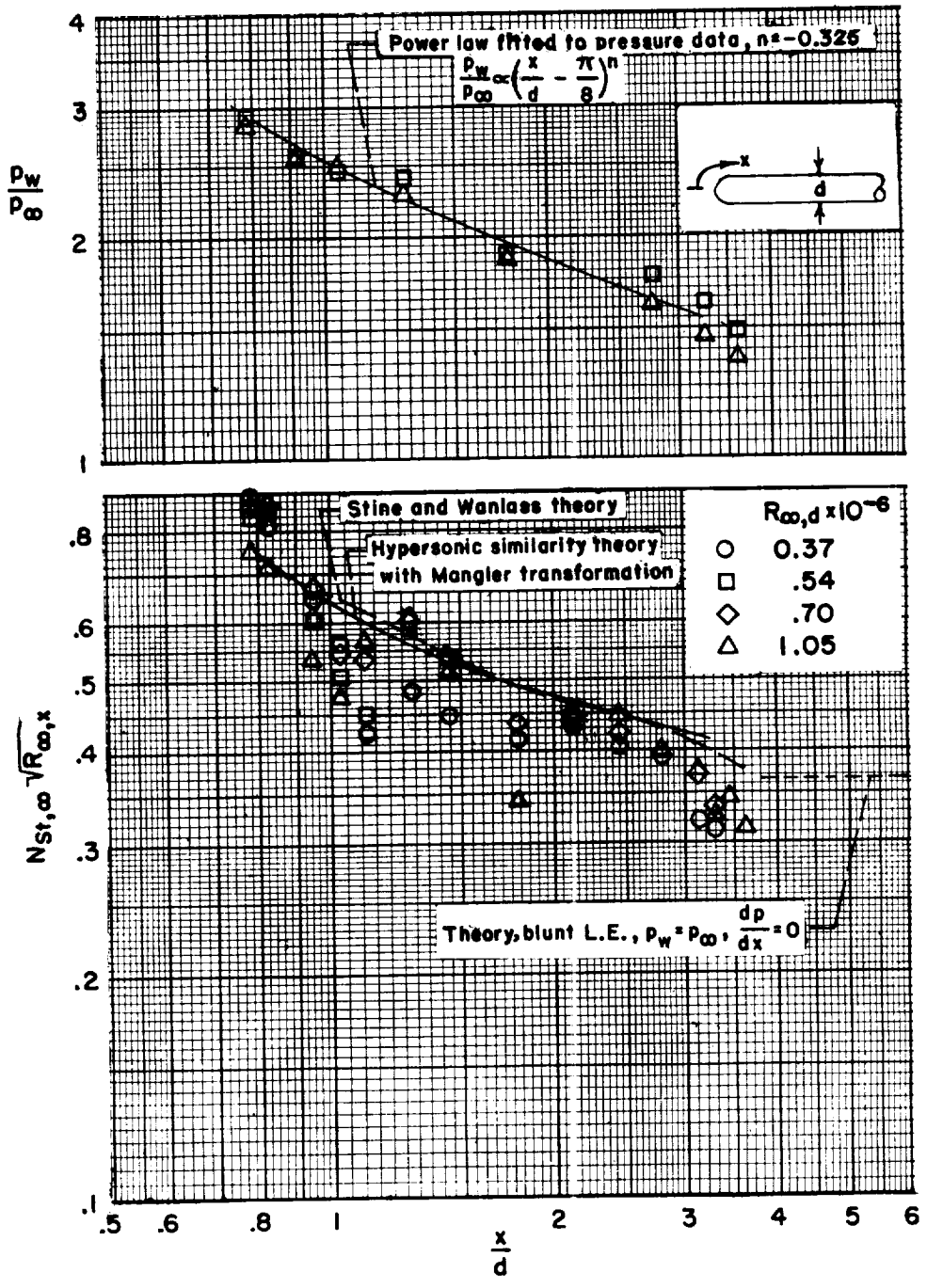

(b) Hemisphere-cylinder, reference 17. $M_\infty = 6.8$.

Figure 11.- Concluded.

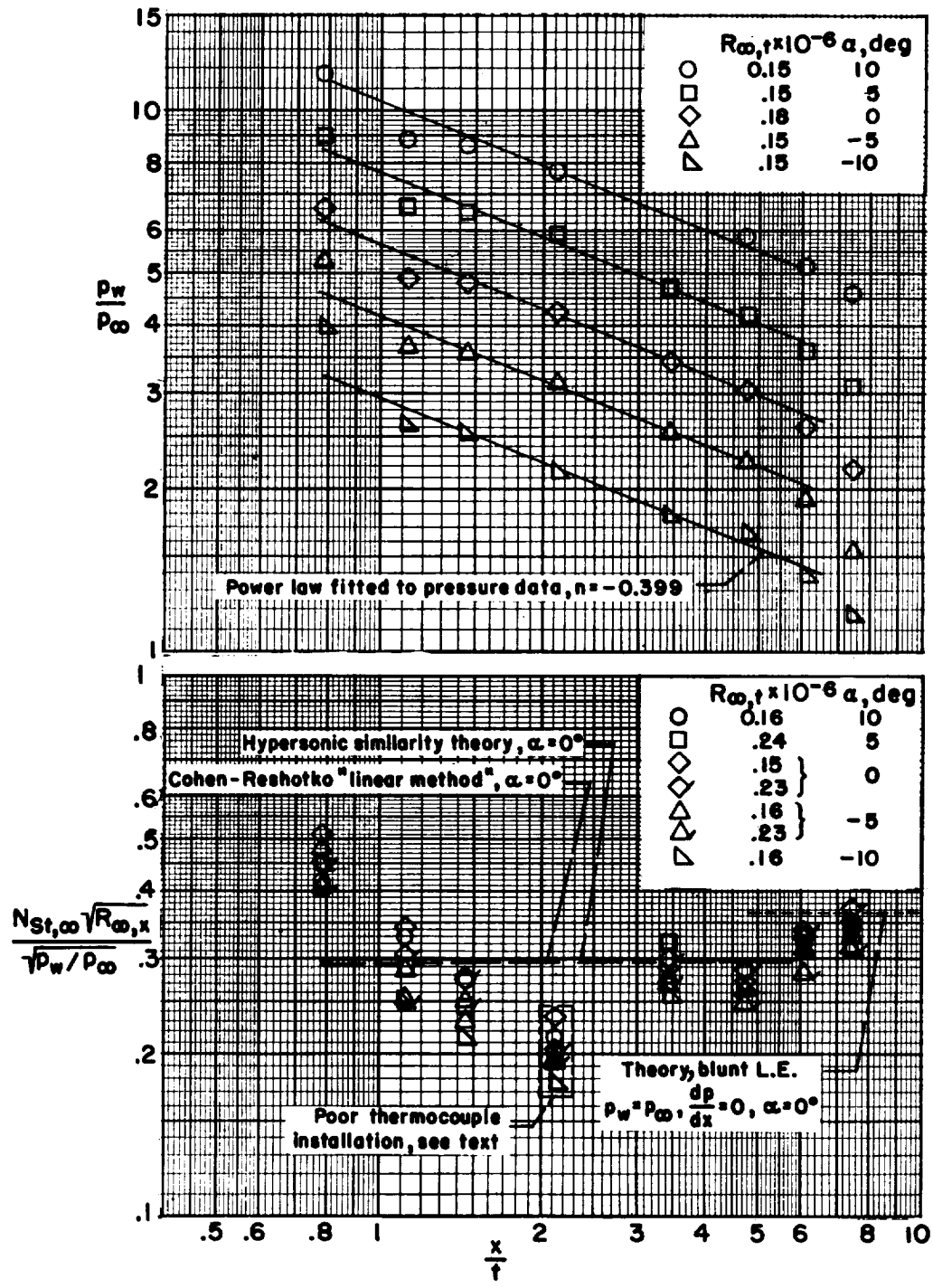

Figure 12.- Comparison of theory with experiment on a hemicylindrical-nose slab at $M_\infty = 6.8$.

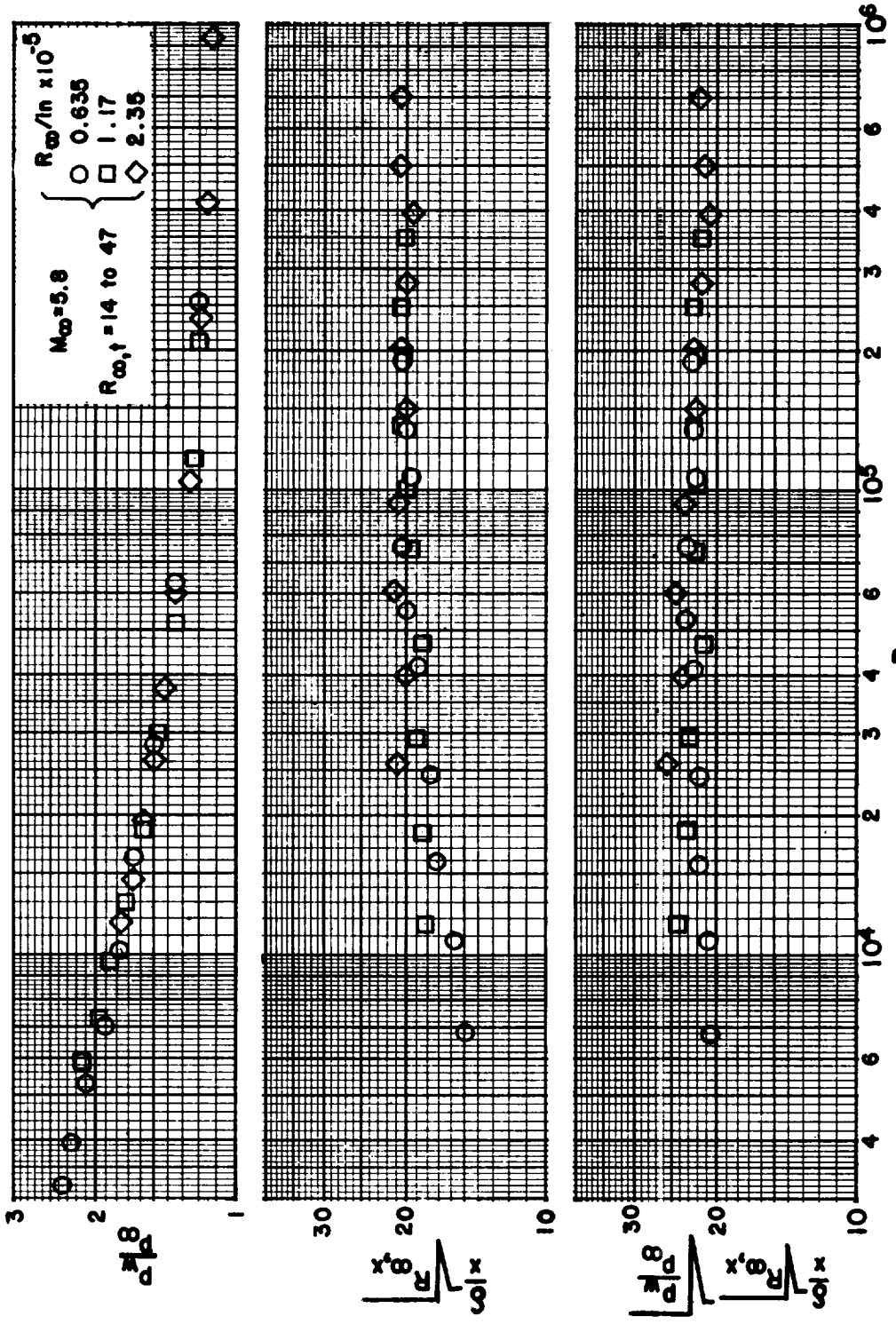

Figure 13.- Effect of local pressure ratio on boundary-layer thickness. Sharp-leading-edge flat plate at zero angle of attack. Data from reference 27.

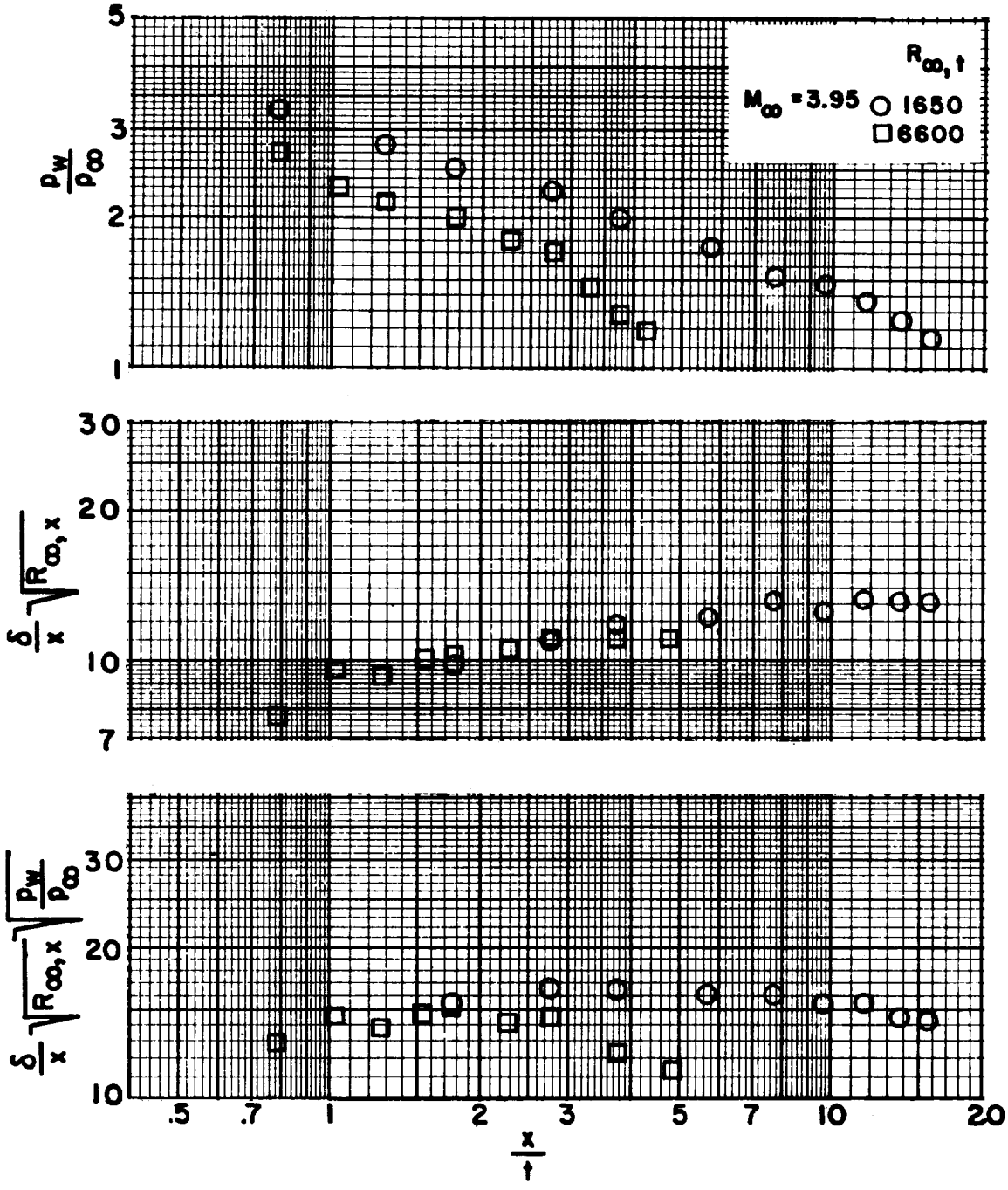

Figure 14.- Effect of local pressure ratio on boundary-layer thickness. Blunt-leading-edge flat plate at zero angle of attack; data from reference 16.

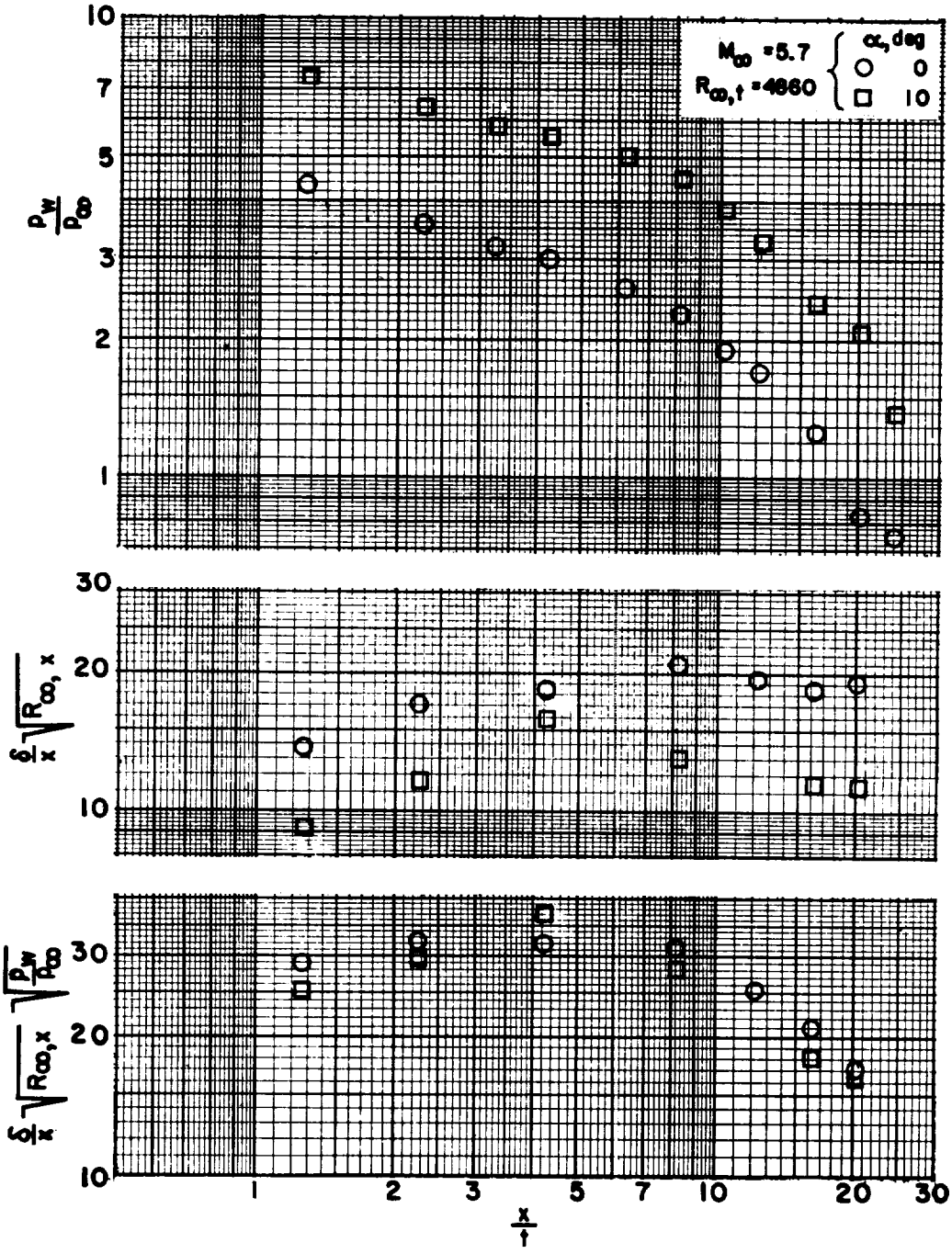

Figure 15.- Effect of local pressure ratio on boundary-layer thickness. Blunt-leading-edge flat plate at two angles of attack; data from reference 28.

NASA - Langley Field, Va. L-185